Distributed MPC of Vehicle Platoons Considering Longitudinal and Lateral Coupling

Yangyang Feng, Shuyou Yu, *Member, IEEE*, Encong Sheng, Yongfu Li, *Senior Member, IEEE*, Shuming Shi, Jianhua Yu, and Hong Chen, *Fellow, IEEE*

***Abstract*— In this paper, a hierarchical control strategy of vehicle platoons is presented, in which the longitudinal and lateral coupling property of vehicles is taken into account. A three-degree-of-freedom dynamic model of vehicles is approximated to a "global" linear model by the Koopman operator theory. A synchronous distributed predictive control scheme of vehicle platoons is proposed as an upper-level controller, where both the linear vehicle model and a linear parametric-varying lane-keeping model are adopted to predict the dynamic of vehicles, and keep vehicles in the designated lane. Thus, it can avoid the solution of nonlinear optimization problems and reduce the computational burden accordingly. A lower-level controller is designed, where the desired longitudinal control force determined by the upper-level controller is transformed into the desired throttle angle and brake pressure through an inverse longitudinal dynamics model of vehicles. The joint simulation results by PreScan, CarSim and MATLAB/Simulink show that when the leader vehicle accelerates or decelerates, the following vehicles in the platoon can keep the same velocity as the leader vehicle, and maintain the desired safety distance between the front and rear vehicles. In addition, joint simulation in the curved road scenario show that the performance of lane keeping can be guaranteed for vehicle platoons with the proposed control strategy.**

***Index Terms*— Vehicle platoon, longitudinal and lateral coupling, Koopman operator, lane-keeping, distributed model predictive control.**

Manuscript received 22 January 2022; revised 25 July 2022, 27 February 2023, and 12 August 2023; accepted 28 September 2023. This work was supported in part by the National Natural Science Foundation of China under Grant U1964202, in part by the Natural Science Foundation of Jilin Province under Grant YDZJ202101ZYTS169, in part by the Foundation of Key Laboratory of Industrial Internet of Things and Networked Control under Grant 2019FF01, and in part by the New Energy Vehicle Power System Key Laboratory in Jiangsu Province under Grant JKLNEVPS201901. The Associate Editor for this article was S. Santini. *(Corresponding author: Shuyou Yu.)*

Yangyang Feng and Encong Sheng are with the Department of Control Science and Engineering, Jilin University, Changchun 130025, China (e-mail: yyfeng19@mails.jlu.edu.cn; shengec20@mails.jlu.edu.cn).

Shuyou Yu is with the State Key Laboratory of Automotive Simulation and Control and the Department of Control Science and Engineering, Jilin University, Changchun 130025, China (e-mail: shuyou@jlu.edu.cn).

Yongfu Li is with the Key Laboratory of Intelligent Air-Ground Cooperative Control for Universities in Chongqing, College of Automation, Chongqing University of Posts and Telecommunications, Chongqing 400065, China (e-mail: liyongfu@ieee.org).

Shuming Shi is with the College of Transportation, Jilin University, Changchun 130025, China (e-mail: shishuming@jlu.edu.cn).

Jianhua Yu is with the Dongfeng Commercial Vehicle Technology Center, Wuhan 430058, China (e-mail: yujh@dfcv.com.cn).

Hong Chen is with the College of Electronics and Information Engineering, Tongji University, Shanghai 200092, China, and also with the Department of Control Science and Engineering, Jilin University, Changchun 130025, China (e-mail: chenh@jlu.edu.cn).

Digital Object Identifier 10.1109/TITS.2023.3323478

NOMENCLATURE

v_i^x	longitudinal velocity of the ith vehicle
v_i^y	lateral velocity of the ith vehicle
$\dot{\psi}_i$	yaw rate of the ith vehicle
I_i^z	inertia moment of the ith vehicle around the z-axis
F_i^{xf}	longitudinal forces of the front tires of the ith vehicle
F_i^{xr}	longitudinal forces of the rear tires of the ith vehicle
F_i^{yf}	lateral forces of the front tires of the ith vehicle
F_i^{yr}	lateral forces of the rear tires of the ith vehicle
a_i	distance from the front axles to mass center of the ith vehicle
b_i	distance from the rear axles to mass center of the ith vehicle
m_i	mass of the ith vehicle
C_i^{cf}	cornering stiffness of the front tires of the ith vehicle
C_i^{cr}	cornering stiffness of the rear tires of the ith vehicle
δ_i	steering angle of the front tires of the ith vehicle
i_s	steering ratio of the ith vehicle
δ_i^f	steering wheel angle of the ith vehicle
$i_{g,i}$	gear ratio of the transmission of the ith vehicle
$i_{o,i}$	ratio of final gear of the ith vehicle
$\eta_{T,i}$	mechanical efficiency of driveline of the ith vehicle
$r_{eff,i}$	effective rolling radius of the wheel of the ith vehicle
$T_{des,i}$	desired engine torque of the ith vehicle
$w_{e,i}$	current engine speed of the ith vehicle

I. INTRODUCTION

CONTROL of connected autonomous vehicle platoons has significant social and economic value for improving vehicle driving safety, energy-saving, and emission reduction [1]. According to the U.S National Highway Traffic Safety Administration, approximately 84% of traffic accidents are caused by driver misoperation. The platooning of autonomous vehicles can significantly reduce driver fatigue, avoid traffic accidents caused by driver misoperation, and greatly improve driving

safety. Moreover, according to the research of the Netherlands Organization for Applied Scientific Research (TNO), vehicle platoon can save 10%∼15% of fuel consumption. In addition, vehicle platoon can increase road traffic capacity, and mitigate traffic congestion. Considering its great potential for energy saving, safety, and high efficiency, control of connected autonomous vehicle platoon has attracted increasing interest in the field of intelligent networked vehicles and intelligent transportation system [2].

The platoon of connected autonomous vehicles is decomposed into four interrelated components in [3]. Under the four-components framework, the vehicle platoon model describes the behavior of each involved vehicle in the platoon [2], [3]. The single integrator model is the simplest vehicle platoon model, in which the position and velocity of vehicles are the state and control input, respectively. In [4], based on the single integrator model, an optimal controller is designed to achieve vehicle platoon driving. In [5], a double-integrator model is established to study the stability and robustness of a vehicle platoon. For the third-order model, the position, velocity, and acceleration of vehicles are chosen as state variables, and the desired acceleration is the control input. In [6], based on the third-order linear model, a hierarchical control scheme is proposed to guarantee platoon stability. However it ignores the longitudinal and lateral dynamics of vehicles. Nonlinear vehicle platoon models cover longitudinal dynamics including engine, transmission, and air resistance, etc [7], [8]. For the vehicle platoon driving on the curved road, not only the longitudinal dynamics but also the lateral dynamics have to be considered. In [9], a two-degree-of-freedom bicycle model is used to describe the lateral dynamics of vehicles, and a model predictive controller is designed to guarantee performance of both longitudinal following and lateral stability of vehicles on the curved road. In [10], a lane-keeping model is adopted to describe the lateral dynamics of vehicles. However, the longitudinal and lateral vehicle dynamics are decoupled in [9] and [10]. It is pointed out in [11] and [12] that the coupled longitudinal and lateral properties of vehicles must be considered for a vehicle platoon driving at high velocities. In this paper, a vehicle platoon model describing the longitudinal and lateral dynamics simultaneously is established, and the coupled longitudinal and lateral control strategy of the vehicle platoon is proposed.

Not only centralized control schemes but also distributed control are widely used in vehicle platoon where a local controller based on vehicle-to-vehicle communication topology is designed for each vehicle, and low computational cost and strong reliability are achieved [13], [14]. In [15], stability of the vehicle platoon with a distributed proportional controller is analyzed when there is a time delay in receiving information from the leader vehicle. Although the design of the distributed proportional controller is simple and easy to implement, it cannot handle constraints and disturbances [16]. Sliding mode controller and H_∞ controller can effectively deal with uncertainties and disturbances of systems. In [17], a distributed sliding mode controller is proposed for vehicle platoons. The sliding mode surface and the control law are designed by a new topological structure function, which enables the strategy to deal with the diversity of information topologies. In [18], a distributed H_∞ control strategy is proposed for heterogeneous vehicle platoon with communication delay, which guarantees robust stability, string stability, and tracking performance. In [19] and [20], a distributed robust PID control scheme is proposed which is able to attenuate uncertainties or disturbances acting on agents. In [21], a distributed model reference adaptive controller is designed to address the containment control problem of heterogeneous uncertain multi-agents system. Distributed model predictive control (DMPC) is widely adopted in vehicle platoons since it can handle constraints, predict future dynamics, and deal with multi-objective optimization problems [22], [23]. In [24], a distributed model predictive controller is designed to achieve consistency and string stability of heterogeneous vehicle platoons. In [25], a dual-mode DMPC scheme is applied to save communication resources, and reduce computational burden. In [26], a DMPC algorithm based on Nash optimality is proposed, where controllers can exchange information during the process of optimization. In [27], a DMPC approach is developed with guaranteed local stability and multi-criteria string stability. In [28], a DMPC algorithm under switching communication topologies and abnormal communications is proposed. The researches mentioned above only investigate the longitudinal tracking control of a vehicle platoon. However, on a curved road, not only longitudinal control, but also lateral control are required in order to achieve safe driving of vehicle platoons [29], [30]. Lateral control approaches of vehicle platoons are usually classified as a lane following approach or a predecessor-vehicle's path following approach [31], [32]. In [32], an integrated longitudinal and lateral control scheme is proposed, where a proportional controller is designed to follow the velocity of the predecessor vehicle and ensure string stability, and a linear time-varying model predictive controller is adopted to achieve the driving path following of the predecessor vehicle. In [33], a distributed longitudinal protocol and a potential function-based distributed lateral control scheme are proposed, which is able to address communication delays and realize merging/splitting maneuvers among platoons. In [34] and [35], a decoupled longitudinal and lateral control strategy is proposed, where a lane keeping controller is designed to keep the vehicle platoon within a designated lane. Furthermore, the longitudinal and lateral control of vehicles in the platoon are considered independently [36], in which coupling characteristics of the longitudinal and lateral dynamics are ignored.

Coupled control of longitudinal and lateral dynamics of autonomous vehicles is a challenging problem. Some researches pay much attention on coupled control of single-vehicles, for example, a nonlinear model predictive control (MPC) algorithm is designed in [37] and [38]. A longitudinal, lateral and vertical integrated control based on nonlinear MPC is proposed in [39] for electric vehicles which takes manipulability, stability and comfort requirements into consideration at the same time. The offset-free MPC is proposed in [40] for coupled longitudinal and lateral motion control of autonomous vehicles. Based on a vehicle kinematic model

considering the longitudinal, lateral and yaw motions, MPC is proposed in [41] to efficiently track the planned trajectory. A novel combined longitudinal and lateral controller based on the unicycle kinematic model is designed in [42] for the hybrid vehicle platoon by introducing a key point sequence matrix. A sliding mode control strategy is proposed in [43] and [44] to effectively handle the coupling and coordination of the longitudinal and lateral motion of vehicles in the platoon. However it cannot deal with constraints, and might produce chattering phenomenon. The coupled control problem of vehicle platoons is studied in [45] and [46] using MPC scheme with the focus on merging control on straight roads. MPC considering a nonlinear vehicle platoon model can lead to nonlinear optimization problems, which will increase the computational burden accordingly [47]. Fortunately, the development of Koopman operator theory [48] provides an approach to describe a finite dimensional nonlinear system with an infinite-dimensional linear system [49]. Dynamic mode decomposition (DMD) algorithm is commonly used to approximate the Koopman operator with a finite dimension matrix [50], [51]. Furthermore, the Koopman operator theory serves as a global linearization method, outperforming local linearization methods in its ability to approximate nonlinear systems [48], [52].

In this paper, a three-degree-of-freedom (3-DOF) dynamic model of vehicles is approximated to a "global" linear model by the Koopman operator theory. Combining the linear model and a lane keeping model, a linear parametric-varying (LPV) vehicle platoon model is established. Then, a synchronous DMPC algorithm is designed. Together with the proposed lower-level controller, performance of longitudinal tracking and lane keeping of the vehicle platoon is verified by the joint simulation based on PreScan, CarSim and Simulink. The main contributions of this paper are as follows:

1) Dynamic mode decomposition of Koopman operator theory is adopted to obtain a "global" linear model of the nonlinear vehicle dynamics. Combining the linear model and the lane keeping model, a linear parametric-varying vehicle platoon model is established.
2) A hierarchical structure with coupled longitudinal and lateral control is proposed for the vehicle platoon. A synchronous DMPC algorithm is proposed as an upper-level controller, where both the linear vehicle model and the linear parametric-varying lane-keeping model are adopted to predict the dynamic of vehicles, and keep vehicles in the designated lane. Thus, the linear approximation can avoid the solution of nonlinear optimization problems and improve computational efficiency, so as to realize the real-time control of the vehicle platoon. Since the desired longitudinal control force calculated by distributed model predictive controller cannot be implemented directly on a real vehicle, a lower-level controller is designed, which transforms the desired longitudinal control force into throttle angle and brake pressure by the inverse longitudinal dynamics model of vehicles.

The rest of the paper is organized as follows. Section II is problem setup, including longitudinal and lateral dynamics of vehicles, Koopman operator for vehicle dynamics, the lane-keeping model, vehicle platoon model, control objective of vehicle platoons. Section III is the design of the coupled longitudinal and lateral control strategy. Section IV is the joint simulation by PreScan, CarSim and MATLAB/Simulink. Section V concludes the paper.

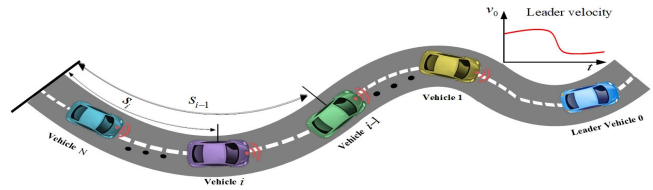

Fig. 1. The vehicle platoon on the curved road.

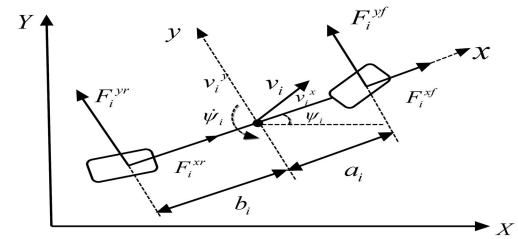

Fig. 2. The 3-DOF bicycle model of vehicles.

II. Problem Setup

Considering a vehicle platoon consists of one leader vehicle and N following vehicles, where the leader vehicle is denoted by 0 and the following vehicles are $1 \cdots N$, respectively. Suppose that the leader vehicle is uncontrollable and maintains its desired motion. The structure of the vehicle platoon on the curved road is shown in Fig. 1.

A. Longitudinal and Lateral Dynamics of Vehicles

For the vehicle platoon driving on the curved road, coordinated control of both longitudinal and lateral motion is required. A 3-DOF bicycle model of vehicles is shown in Fig. 2, which includes longitudinal, lateral, and yaw motions.

The mechanical equation of the longitudinal, lateral, and yaw motion of the ith vehicle is [53]:

$$\begin{cases} (m_i \dot{v}_i^x - m_i \dot{v}_i^y \dot{\psi}_i) = F_i{}^{xf} + F_i{}^{xr} \\ (m_i \dot{v}_i^y + m_i \dot{v}_i^x \dot{\psi}_i) = F_i{}^{yf} + F_i{}^{yr} \\ I_i^z \ddot{\psi}_i = a_i F_i{}^{yf} - b_i F_i{}^{yr} \end{cases} \tag{1}$$

where $i \in 1, 2, \ldots, N$.

Assume that the slip angles of front and rear tires are within a small range [54], and the model of tires is linear, i.e., the lateral force of front and rear tires are

$$\begin{aligned} F_i{}^{yf} &= C_i^{cf}(\delta_i - \frac{v_i^y + a_i \dot{\psi}_i}{v_i^x}) \\ F_i{}^{yr} &= C_i^{cr}(\frac{b_i \dot{\psi}_i - v_i^y}{v_i^x}) \end{aligned} \tag{2}$$

Set $F_i^x = F_i^{xf} + F_i^{xr}$. The vehicle dynamic model of longitudinal and lateral coupling is as follows:

$$\begin{cases} \dot{v}_i^x = v_i^y \dot{\psi}_i + \dfrac{1}{m_i} F_i^x \\ \dot{v}_i^y = -v_i^x \dot{\psi}_i + \dfrac{1}{m_i}\Big(-\dfrac{(C_i^{cf} + C_i^{cr})v_i^y}{v_i^x} - \dfrac{(C_i^{cf} a_i - C_i^{cr} b_i)\dot{\psi}_i}{v_i^x} \\ \qquad\qquad + C_i^{cf}\delta_i\Big) \\ \ddot{\psi}_i = \dfrac{1}{I_i^z}\Big(-\dfrac{(C_i^{cf} a_i - C_i^{cr} b_i)v_i^y}{v_i^x} - \dfrac{(C_i^{cf} a_i^2 + C_i^{cr} b_i^2)\dot{\psi}_i}{v_i^x} \\ \qquad\qquad + C_i^{cf} a_i \delta_i\Big) \end{cases} \tag{3}$$

Define the state as $x_i = [v_i^x \;\; v_i^y \;\; \dot{\psi}_i]^T$ and the control input as $u_i = [F_i^x \;\; \delta_i]^T$. Rewrite the 3-DOF bicycle model (3) as:

$$\dot{x}_i = f\left(x_i, u_i\right) \tag{4}$$

where function $f : \mathbb{R}^3 \times \mathbb{R}^2 \longrightarrow \mathbb{R}^3$ represents the nonlinear mapping of (3).

B. Koopman Operator for Vehicle Dynamics

The basic idea of the Koopman operator theory is to convert a nonlinear dynamics system into a linear system in a new space [48], [49]. Denote T_s as the sampling time. Then, with a little abuse of notation, the discrete counterpart of (4) is rewritten as

$$x_{k+1,i} = f\left(x_{k,i}, u_{k,i}\right) \tag{5}$$

where $x_{k,i} \in \mathbb{R}^3$ and $u_{k,i} \in \mathbb{R}^2$ are the state and control input of the ith vehicle at time instant k.

Define κ as the Koopman operator acting on the observation function $\varphi\left(x_{k,i}\right)$, i.e.,

$$\kappa\varphi\left(x_{k,i}\right) = \varphi\left(x_{k+1,i}\right) = \varphi\left(f(x_{k,i})\right) \tag{6}$$

where $\varphi\left(x_{k,i}\right)$ is also referred to as a Koopman eigenfunction [55].

DMD algorithm can be adopted to approximate the Koopman operator κ [50], [51]. In DMD algorithm, the input and output data matrix are comprised of p snapshots which each from the nonlinear vehicle dynamics (5), i.e.,

$$\begin{aligned} X_i^D &= \left[\, x_{1,i} \;\; x_{2,i} \;\; \cdots \;\; x_{p,i} \,\right] \\ \Upsilon_i &= \left[\, u_{1,i} \;\; u_{2,i} \;\; \cdots \;\; u_{p,i} \,\right] \\ Y_i^D &= \left[\, x_{2,i} \;\; x_{3,i} \;\; \cdots \;\; x_{p+1,i} \,\right] \end{aligned} \tag{7}$$

where $X_i^D \in \mathbb{R}^{3\times p}$, $Y_i^D \in \mathbb{R}^{3\times p}$, $\Upsilon_i \in \mathbb{R}^{2\times p}$, p is the total number of snapshots.

The linear approximation of the nonlinear dynamics (5) can be written as

$$Y_i^D = A_i^D X_i^D + B_i^D \Upsilon_i = \left[A_i^D \;\; B_i^D\right]\begin{bmatrix} X_i^D \\ \Upsilon_i \end{bmatrix} = \Psi_i \Omega_i \tag{8}$$

where $A_i^D \in \mathbb{R}^{3\times 3}$, $B_i^D \in \mathbb{R}^{3\times 2}$, $\Psi_i = \left[A_i^D \;\; B_i^D\right]$, and $\Omega_i = \left[X_i^D \;\; \Upsilon_i\right]^T$. The best-fit linear operator $\Psi_i = \left[A_i^D \;\; B_i^D\right]$ can be obtained by solving a least-squares optimization problem:

$$\underset{\Psi_i}{minmize} \left\| Y_i^D - \Psi_i \Omega_i \right\|_F \tag{9}$$

where $\|\cdot\|_F$ denotes the Frobenius norm [56]. The matrix Ψ_i can be approximated by

$$\Psi_i = Y_i^D \Omega_i^\dagger \tag{10}$$

where $\Omega_i^\dagger$ is the Moore-Penrose pseudoinverse of Ω_i. Apply Singular Value Decomposition (SVD) of matrix Ω_i, i.e.,

$$\Omega_i = U \Sigma V^T \tag{11}$$

where $U \in \mathbb{R}^{5\times 5}$ and $V^T \in \mathbb{R}^{5\times p}$ are orthogonal matrices, $\Sigma \in \mathbb{R}^{5\times 5}$ is a diagonal matrix. Then, (10) can be rewritten as

$$\Psi_i = Y_i^D V \Sigma^{-1} U^T \tag{12}$$

In practice, we can improve the computational efficiency by truncation of the expression $\Omega_i = U\Sigma V^T$, and obtain an approximation

$$\Omega_i \approx U_{\tilde{r}} \Sigma_{\tilde{r}} V_{\tilde{r}}^T$$

where $U_{\tilde{r}} \in \mathbb{R}^{5\times r}$, $\Sigma_{\tilde{r}} \in \mathbb{R}^{r\times r}$, and $V_{\tilde{r}}^T \in \mathbb{R}^{r\times p}$ are truncated matrices. The parameter r is chosen as $r = 3$ in this paper. Accordingly, Ψ_i of (10) can be approximated as

$$\tilde{\Psi}_i = Y_i^D V_{\tilde{r}} \Sigma_{\tilde{r}}^{-1} U_{\tilde{r}}^T \tag{13}$$

Similarly, A_i^D and B_i^D can be computed by the following equations:

$$\begin{aligned} A_i^D &\approx Y_i^D V_{\tilde{r}} \Sigma_{\tilde{r}}^{-1} U_{\tilde{r},1}^T \\ B_i^D &\approx Y_i^D V_{\tilde{r}} \Sigma_{\tilde{r}}^{-1} U_{\tilde{r},2}^T \end{aligned} \tag{14}$$

where $U_{\tilde{r}} = [U_{\tilde{r},1} \;\; U_{\tilde{r},2}]^T$, $U_{\tilde{r},1} \in \mathbb{R}^{3\times r}$, $U_{\tilde{r},2} \in \mathbb{R}^{2\times r}$.

Thus, the discrete linear model of vehicles can be constructed as

$$x_{k+1,i} = A_i^D x_{k,i} + B_i^D u_{k,i} \tag{15}$$

Note that the linear model (15) obtained by the DMD algorithm remains the same number of dimensions as the original system (5) [50], [51].

To verify the effectiveness of the linear vehicle model approximated by the Koopman operator theory, the dataset of the vehicle dynamics model (4) must be obtained first. Set the sampling time $T_s = 0.1$s, and discretize (4) using the Runge-Kutta method. Two simulation experiments are set to compare the evolution of states of the nonlinear system (4) and the linear system (15) approximated by the Koopman operator theory.

- Scenario 1: The initial state of $[v_i^x \;\; v_i^y \;\; \dot{\psi}_i] = [20 \;\; 0 \;\; 0]$. The states are uniformly sampled in the interval: $v_i^x \in [5 \;\; 30]$, $v_i^y \in [-1 \;\; 1]$, and $\dot{\psi}_i \in [-0.5 \;\; 0.5]$, while the inputs are uniformly sampled in the interval $F_i^x \in [-4000 \;\; 4000]$ and $\delta_i \in [-0.1 \;\; 0.1]$.
- Scenario 2: The initial state of $[v_i^x \;\; v_i^y \;\; \dot{\psi}_i] = [20 \;\; 0 \;\; 0]$. The longitudinal force F_i^x is set to 3000N, and the steering angle of the front tires is $\delta_i = 0.1sin(0.4\pi t)$.

Furthermore, the average Root Mean Square Error (RMSE) is calculated as an objective evaluation index [48], i.e.,

$$RMSE = \frac{\sqrt{\sum_k \left\| x_{nonl}(k) - x_{koop}(k) \right\|_2^2}}{\sqrt{\sum_k \left\| x_{nonl}(k) \right\|_2^2}} \times 100\% \tag{16}$$

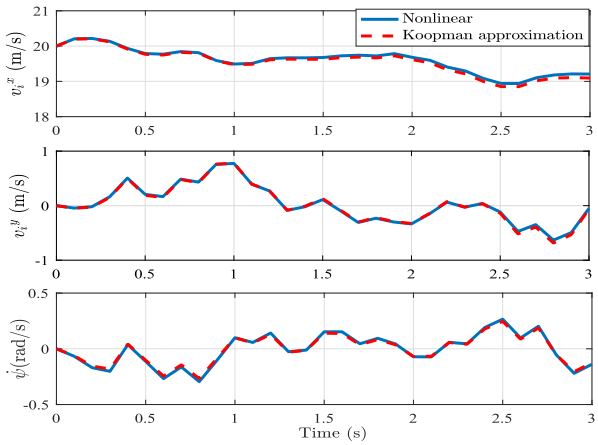

Fig. 3. Validation of the linear model approximated by the Koopman operator theory (Scenario 1).

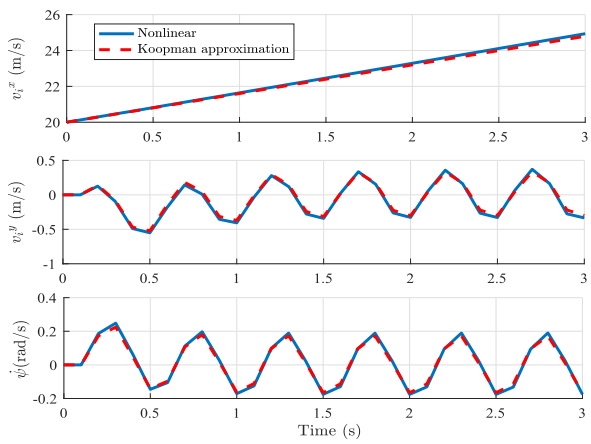

Fig. 4. Validation of the linear model approximated by the Koopman operator theory (Scenario 2).

where $x_{nonl}(k)$ and $x_{koop}(k)$ are states obtained at time instant k from the nonlinear vehicle dynamics model (4) and the linear model (15), respectively. Fig. 3 and Fig. 4 show the experiment results of the nonlinear system (4) and the linear system (15) under the two scenarios, respectively. Accordingly, the values of the average RMSE under the two scenarios are 0.31% and 0.39%, respectively. It can be found that the linear model developed by the Koopman operator theory can accurately approximate nonlinear vehicle dynamics.

C. The Lane-Keeping Model

Suppose that the leader vehicle is uncontrolled, cf. its position and velocity are given as s_0 and v_0^x *a priori*. For each vehicle i, $i \in 1, 2, \ldots, N$ describe its position as s_i, and define its spacing error as

$$e_i^p = s_i - (s_0 - i d_{des})$$

where d_{des} is the desired distance between the front and rear vehicles.

In this paper, the constant distance policy [57] is chosen

$$d_{des} = d_0 \tag{17}$$

with $d_0 > 0$.

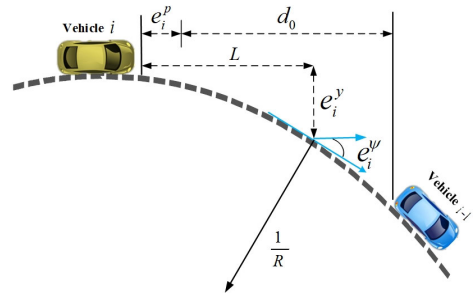

Fig. 5. The structure of the lane-keeping model.

In order to make vehicles run along both a curved or straight road, a lane-keeping model is taken into account [43], [44], [58]. The structure of the lane-keeping model is shown in Fig. 5.

Denote the heading error of vehicle i relative to a lane as

$$e_i^\psi = \psi_i^d - \psi_i$$

where ψ_i and ψ_i^d are the actual vehicle heading angle and the tangential angle of the desired lane, respectively.

Denote lateral position error from the mass center of the ith vehicle to the center of lane as e_i^y. Then one has

$$\begin{cases} \dot{e}_i^p = v_i^x - v_0^x \\ \dot{e}_i^y = v_i^x e_i^\psi - v_i^y - L\dot{\psi}_i \\ \dot{e}_i^\psi = \dot{\psi}_i^d - \dot{\psi}_i \end{cases} \tag{18}$$

where $\dot{\psi}_i^d$ is the desired yaw rate, i.e.,

$$\dot{\psi}_i^d = \frac{v_i^x}{R}$$

The term R is the radius of the road, which is time-varying. The term L is the specified look-ahead distance.

Assumption 1: The leader vehicle is uncontrolled, however, its position s_0 and velocity v_0^x are assumed to be known. In addition, both the road radius R and the specified look-ahead distance L are also assumed to be known.

Remark 1: In principle, (18) is an autonomous system, where v_0^x and $\dot{\psi}_i^d$ are reference signals. If v_i^x, v_i^y and $\dot{\psi}_i$ are treated as "input", (18) is a bilinear system; if v_i^x, v_i^y and $\dot{\psi}_i$ are treated as varying parameters, (18) is a linear parametric-varying system.

D. Vehicle Platoon Model for Control

Combine (15) and (18), and define the state

$$X_i(k) = \left[v_i^x(k) \;\; v_i^y(k) \;\; \dot{\psi}_i(k) \;\; e_i^p(k) \;\; e_i^y(k) \;\; e_i^\psi(k)\right]^T$$

The control inputs are the desired longitudinal control force, and the steering angle of the front tires, respectively

$$U_i(k) = \left[F_i^x(k) \;\; \delta_i(k)\right]^T$$

Then, a discrete linear parametric-varying model describing the longitudinal and lateral dynamics is

$$X_i(k+1) = A_i\left(v_i^x(k)\right) X_i(k) + B_i U_i(k) + E_i w_i(k) \tag{19}$$

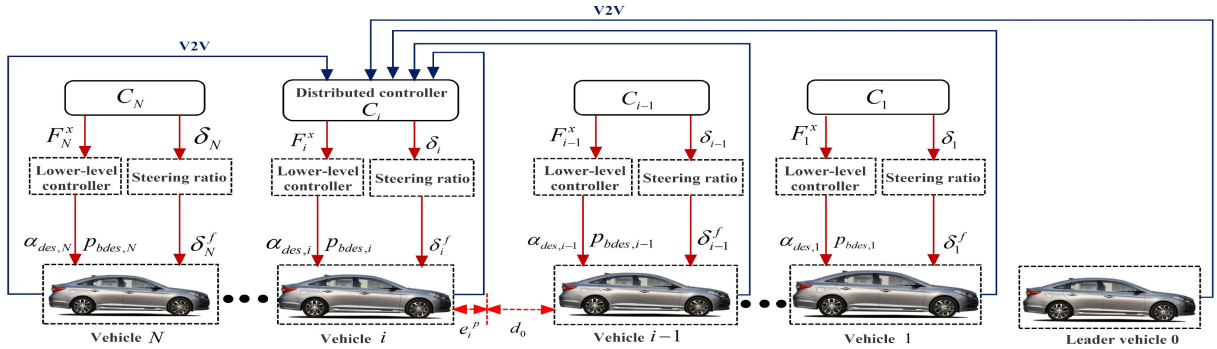

Fig. 6. The distributed control framework of the vehicle platoon.

where

$$A_i\left(v_i^x(k)\right) = \left[\begin{array}{ccc|ccc} \multicolumn{3}{c|}{A_i^D} & \multicolumn{3}{c}{0_{3\times3}} \\ \hline T_s & 0 & 0 & 1 & 0 & 0 \\ 0 & -T_s & -T_sL & 0 & 1 & T_s v_i^x(k) \\ 0 & 0 & -T_s & 0 & 0 & 1 \end{array}\right]$$

$$E_i = \begin{bmatrix} 0_{3\times2} \\ \hline -T_s & 0 \\ 0 & 0 \\ 0 & T_s \end{bmatrix} \quad B_i = \begin{bmatrix} B_i^D \\ \hline 0_{3\times2} \end{bmatrix} \quad w_i(k) = \begin{bmatrix} v_0^x(k) \\ \dot{\psi}_i^d(k) \end{bmatrix}$$

Note that the system matrix $A_i\left(v_i^x(k)\right)$ depends on the time-varying parameter $v_i^x \in \left[v_{i,min}^x \;\; v_{i,max}^x\right]$, where $v_{i,min}^x$ and $v_{i,max}^x$ are the minimum and maximum longitudinal velocity of the ith vehicle. Denote the matrices $A_i^{min}\left(v_i^x(k)\right)$, $A_i^{max}\left(v_i^x(k)\right)$ as

$$\begin{cases} A_i^{min}\left(v_i^x(k)\right) = A_i\left(v_i^x(k)\right)|_{v_i^x = v_{i,min}^x} \\ A_i^{max}\left(v_i^x(k)\right) = A_i\left(v_i^x(k)\right)|_{v_i^x = v_{i,max}^x} \end{cases}$$

The system matrix $A_i\left(v_i^x(k)\right)$ belongs to a polytope Ω_i, i.e.,

$$\Omega_i := Con\left\{A_i^{min}\left(v_i^x(k)\right),\; A_i^{max}\left(v_i^x(k)\right)\right\}$$

where $Con\{\cdot\}$ is a convex hull of matrices.

Remark 2: The model (19) describes the longitudinal and lateral dynamic characteristics of vehicles in the platoon, i.e., the vehicle in the platoon maintains within the designated lane.

Remark 3: It is also feasible to directly obtain an LPV model from a nonlinear vehicle platoon model. However, if the direct LPV model is adopted, which will depend on the time-varying parameters of $\{v_i^y \in [v_{i,min}^y \; v_{i,max}^y]$, $v_i^x \in [v_{i,min}^x \; v_{i,max}^x]$, $\frac{1}{v_i^x} \in [1/v_{i,max}^x \; 1/v_{i,min}^x]\}$. Furthermore, a polytope linear differential inclusions (LDI) of the direct LPV model can be described as $\Omega_i := Con\{[A_1 \; B_1], [A_2 \; B_2], \ldots, [A_M \; B_M]\}$, where $M \geq 8$, which might cause the obtained terminal set to be more conservative [59], [60].

Remark 4: Since the longitudinal and lateral characteristic of the vehicle in the platoon depends strongly on reference signals v_0^x and the radius of the road R, it is difficult to obtains its "global" linear model directly by the Koopman operator theory.

Remark 5: The matrix $A_i\left(v_i^x(k)\right)$, $i \in [1, \; N]$, is a lower triangular matrix, i.e., e_i^p, e_i^y and e_i^ψ have no direct influence on v_i^x, v_i^y and $\dot{\psi}_i$.

E. Control Objective of Vehicle Platoon

The longitudinal control objective of the vehicle platoon is to track the longitudinal velocity of the leader vehicle, and to force the inter-vehicle spacing errors converge to zero, i.e.,

$$\begin{cases} minimize \left\|v_i^x(k) - v_0^x(k)\right\|_2^2 \\ minimize \left\|e_i^p(k) - 0\right\|_2^2 \end{cases} \tag{20}$$

where $\|\vartheta(k)\|_2$ defines as the 2-norm of the function $\vartheta(k)$, i.e., $\|\vartheta(k)\|_2 := \sqrt{\sum_{k=0}^{\infty}(\vartheta(k))^2} < \infty$, and $\lim_{k\to\infty} \vartheta(k) = 0$.

In order to avoid collision of vehicles in the platoon, a collision avoidance constraint is designed

$$e_{i,min}^p \leq e_i^p(k) \leq e_{i,max}^p \tag{21}$$

where $e_{i,max}^p$ and $e_{i,min}^p$ are the maximum and minimum spacing errors.

The lateral control objective is that vehicles in the platoon runs as close as possible to the centerline of the road, i.e.,

$$\begin{cases} minimize \left\|e_i^y(k) - 0\right\|_2^2 \\ minimize \left\|e_i^\varphi(k) - 0\right\|_2^2 \end{cases} \tag{22}$$

Furthermore, in order to guarantee that vehicles in the platoon do not go beyond the road boundary, the following constraints are required to be satisfied

$$\begin{cases} e_i^\psi(k) \in \left[e_{i,min}^\psi \quad e_{i,max}^\psi\right] \\ e_i^y(k) \in \left[e_{i,min}^y \quad e_{i,max}^y\right] \end{cases} \tag{23}$$

where $e_{i,min}^\psi$ and $e_{i,max}^\psi$ are the allowed minimum and maximum heading errors of vehicle i relative to lane; $e_{i,min}^y$ and $e_{i,max}^y$ are the minimum and maximum lateral position errors relative to lane.

III. Coupled Longitudinal and Lateral Control

A distributed control framework shown in Fig. 6 is adopted for vehicle platoons, where each vehicle except for the leader vehicle is controlled only using neighbouring information. In Fig. 7, a hierarchical structure with coupled longitudinal

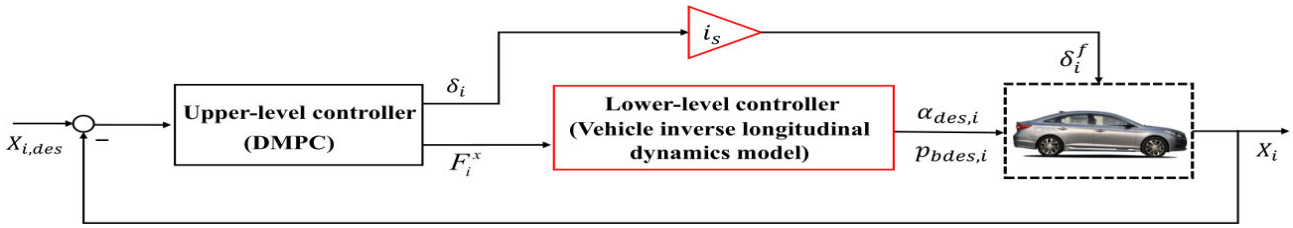

Fig. 7. The hierarchical structure with coupled longitudinal and lateral control.

and lateral control is proposed for each vehicle, where the upper-level controller is a synchronous distributed model predictive controller to achieve control objectives of the vehicle platoon. Since the desired longitudinal control force F_i^x calculated by the upper-level controller cannot be implemented directly on the real vehicle, a lower-level controller is designed, which transforms the desired longitudinal control force into throttle angle and brake pressure by an inverse longitudinal dynamics model of the vehicle. In Fig. 7, X_i is the state of the ith vehicle; $X_{i,des}$ is the desired reference of the ith vehicle; i_s is the steering ratio of the vehicle, which is defined as the ratio between the input angle of the steering wheel and the output angle of the front tires; δ_i^f is the steering wheel angle; $\alpha_{des,i}$ is the desired throttle angle; $p_{bdes,i}$ is the desired brake pressure.

A. Distributed Model Predictive Controller

Under the DMPC framework, a global optimization problem is transformed into a local optimization problem of each vehicle, i.e., all the following vehicles solve its own optimization problem synchronously.

According to (19), the reference of the following vehicles in the platoon is

$$X_{i,des}(k) = \left[v_{i,des}^x(k)\ \ v_{i,des}^y(k)\ \ \dot{\psi}_i^d(k)\ \ e_{i,des}^p(k)\ \ e_{i,des}^y(k)\ \ e_{i,des}^\psi(k)\right]^T \tag{24}$$

where

(i) $v_{i,des}^x(k)$ is the desired longitudinal velocity of the ith vehicle. In order to guarantee that the vehicle in the platoon can track the longitudinal velocity of the leader vehicle, set $v_{i,des}^x(k) = v_0^x$.

(ii) $v_{i,des}^y(k)$ is the desired lateral velocity of the ith vehicle. Since a larger lateral velocity can result in handling stability problem of vehicles in the platoon, set $v_{i,des}^y(k) = 0$, i.e., restrict the lateral velocity as small as possible.

(iii) $e_{i,des}^p(k)$ is the desired spacing error of the ith vehicle. In order to minimize the spacing error, set $e_{i,des}^p(k) = 0$.

(iv) $e_{i,des}^\psi(k)$ and $e_{i,des}^y(k)$ are the desired heading error and lateral position error, respectively. In order to guarantee that the vehicle in the platoon runs as close as possible to the centerline of the road, set $e_{i,des}^\psi(k) = 0$ and $e_{i,des}^y(k) = 0$.

Assumption 2: All the following vehicles share a synchronized clock, i.e., time synchronization is guaranteed.

Note that vehicle-to-vehicle communication delays are very insignificant ($\approx$ 10ms), which can be negligible for a small vehicle platoon [27], [61]. The vehicle-to-vehicle communication topology can be represented by a directed graph $\mathbb{G} = \{\mathbb{V}, \mathbb{E}\}$, where $\mathbb{V} = \{0, 1, 2, \ldots, N\}$ represents the set of vehicles, and $\mathbb{E} \subseteq \mathbb{V} \times \mathbb{V}$ represents the set of edges in connection of vehicles [7]. Furthermore, define $\mathcal{A} = [a_{i\tilde{j}}] \in \mathbb{R}^{N\times N}$ as the adjacency matrix, which is utilized to describe the information interchange between any two vehicles. That is

$$\mathcal{A} = [a_{i\tilde{j}}] = \begin{cases} a_{i\tilde{j}} = 1, & \text{if } \{\tilde{j}, i\} \in \mathbb{E} \\ a_{i\tilde{j}} = 0, & \text{if } \{\tilde{j}, i\} \notin \mathbb{E} \end{cases} \tag{25}$$

where $i, \tilde{j} \in \mathbb{V}$ and $\{\tilde{j}, i\} \in \mathbb{E}$ represents a directional edge from vehicle $\tilde{j}$ to vehicle i. Define $\mathbb{N}_i = \{\tilde{j}\,|a_{i\tilde{j}} = 1,\ \tilde{j} \in 1, 2, \ldots, N\}$ as the neighbor set of the vehicle i, i.e., vehicle i can receive information from each vehicle $\tilde{j} \in \mathbb{N}_i$. Also, define $\Theta_i = \{\tilde{j}\,|a_{\tilde{j}i} = 1,\ \tilde{j} \in 1, 2, \ldots, N\}$, which means that the vehicle i can send the information to each vehicle $\tilde{j} \in \Theta_i$.

For each vehicle i, define the sequence of control inputs as

$$U_i(:|k) = \{U_i(0|k),\ U_i(1|k), \ldots,\ U_i(N_p - 1|k)\}$$

where N_p is the prediction horizon. Accordingly, the state trajectory is denoted as

$$X_i(:|k) = \{X_i(0|k),\ X_i(1|k), \ldots,\ X_i(N_p|k)\}$$

The desired reference trajectory is defined as

$$X_{i,des}(j|k) = \left[v_{i,des}^x(k)\ \ v_{i,des}^y(k)\ \ \dot{\psi}_i^d(j|k)\ \ e_{i,des}^p(k)\ \ e_{i,des}^y(k)\ \ e_{i,des}^\psi(k)\right]^T$$

where $j = 1, \ldots, N_p$, $X_{i,des}(0|k) = X_{i,des}(k)$, $\dot{\psi}_i^d(j|k) = \frac{v_i^x(j|k)}{R}$. Note that the radius of the road R is in principle time-varying, and the heading error $e_i^\psi(k)$ is caused by the variation of the road curvature $\frac{1}{R}$. Assume that the road curvature $\frac{1}{R}$ can be measured within the preview distance L by vehicle-to-road equipments. Furthermore, the preview distance L satisfies $L \geq N_p * T_s * v_{i,max}^x$ for all $i = 1, 2, \ldots, N$ to ensure the "measurement" of the heading error $e_i^\psi(k)$ of vehicle i relative to lane within the prediction horizon.

Denote

$$\tilde{y}_i(j|k) = \tilde{C}_i X_i(j|k), \quad j = 0, 1, \ldots, N_p$$

with $\tilde{C}_i = \text{diag}(1, 0, 0, 1, 0, 0)$ as the predicted output trajectory in the longitudinal direction.

The optimization problem of each vehicle is as follows

Problem 1

$$\underset{U_i(:|k)}{minimize}\ J_i\left(X_i(:|k), U_i(:|k), \tilde{y}_i(:|k), \hat{\tilde{y}}_i(:|k), \hat{\tilde{y}}_{\tilde{j}}(:|k)\right) \tag{26a}$$

$$\text{subject to}\quad X_i(j+1|k) = A_i\left(v_i^x(k)\right)X_i(j|k) + B_iU_i(j|k) + E_iw_i(j|k) \tag{26b}$$

$$X_i(0|k) = X_i(k) \tag{26c}$$

$$F_{i,min}^x \le F_i^x(j|k) \le F_{i,max}^x \tag{26d}$$

$$\delta_{i,min} \le \delta_i(j|k) \le \delta_{i,max} \tag{26e}$$

$$v_{i,min}^x \le v_i^x(j|k) \le v_{i,max}^x \tag{26f}$$

$$v_{i,min}^y \le v_i^y(j|k) \le v_{i,max}^y \tag{26g}$$

$$\dot{\psi}_{i,min} \le \dot{\psi}_i(j|k) \le \dot{\psi}_{i,max} \tag{26h}$$

$$e_{i,min}^p \le e_i^p(j|k) \le e_{i,max}^p \tag{26i}$$

$$e_{i,min}^\psi \le e_i^\psi(j|k) \le e_{i,max}^\psi \tag{26j}$$

$$e_{i,min}^y \le e_i^y(j|k) \le e_{i,max}^y \tag{26k}$$

$$\left(X_i(N_p|k) - X_{i,des}(N_p|k)\right) \in \mathbb{X}_i^f \tag{26l}$$

where

$$\begin{aligned} &J_i\left(X_i(:|k), U_i(:|k), \tilde{y}_i(:|k), \hat{\tilde{y}}_i(:|k), \hat{\tilde{y}}_{\tilde{j}}(:|k)\right) \\ &= \sum_{j=0}^{N_p-1}\Big\{\left\|X_i(j|k)-X_{i,des}(j|k)\right\|_{Q_i}+\left\|\tilde{y}_i(j|k)-\hat{\tilde{y}}_i(j|k)\right\|_{G_i} \\ &\quad + \sum_{\tilde{j}\in\mathbb{N}_i}\left\|\tilde{y}_i(j|k)-\hat{\tilde{y}}_{\tilde{j}}(j|k)\right\|_{F_i} + \left\|U_i(j|k)\right\|_{R_i}\Big\} \\ &\quad + \left\|X_i(N_p|k) - X_{i,des}(N_p|k)\right\|_{P_i} \end{aligned} \tag{27}$$

In prediction horizon $[0\ N_p-1]$, three types of control input trajectories are defined

- $U_i(j|k)$: the predicted control input trajectory
- $\hat{U}_i(j|k)$: the assumed control input trajectory
- $U_i^*(j|k)$: the optimal control input trajectory.

Accordingly, three types of state trajectories are denoted

- $X_i(j|k)$: the predicted state trajectory
- $\hat{X}_i(j|k)$: the assumed state trajectory
- $X_i^*(j|k)$: the optimal predicted state trajectory.

In Problem 1, Q_i, G_i, F_i, and R_i are positive definite weight matrices to be determined. The term P_i is the terminal penalty matrix. Note that $\|\sigma_i\|_{Q_i} = \sigma_i^T Q_i \sigma_i$ with $Q_i \in \mathbb{R}^{n\times n}$ and $Q_i > 0$ for a vector $\sigma_i \in \mathbb{R}^n$. The terminal cost function $\|X_i(N_p|k) - X_{i,des}(N_p|k)\|_{P_i}$ and the terminal set $\mathbb{X}_i^f$ are adopted to guarantee asymptotic consensus of the vehicle platoon. The term $\hat{\tilde{y}}_i(j|k)$ is the assumed output trajectory of the ith vehicle. The term $\hat{\tilde{y}}_{\tilde{j}}(j|k)$ is the assumed output trajectory transmitted from neighboring vehicle.

Note that for the linear parametric-varying system (19), there exists a state feedback control law $U_i(k) = K_iX_{i,e}(k)$ such that $A_i^k := A_i\left(v_i^x(k)\right) + B_iK_i$ is asymptotically stable, where $X_{i,e}(k) = X_i(k) - X_{i,des}(k)$, i.e., the linear parametric-varying system (19) is controllable.

The assumed control sequence $\hat{U}_i(j|k)$ is constructed

$$\hat{U}_i(j|k) = \begin{cases} U_i^*(j+1|k-1), & j=0,\cdots,N_p-2 \\ K_i(X_i(N_p|k-1)-X_{i,des}(N_p|k-1)), & j=N_p-1 \end{cases} \tag{28}$$

Apply the assumed control sequence, and calculate the corresponding assumed output trajectory

$$\begin{cases} \hat{X}_i(j+1|k) = A_i\left(v_i^x(k)\right)\hat{X}_i(j|k) + B_i\hat{U}_i(j|k) + E_iw_i(j|k) \\ \hat{\tilde{y}}_i(j|k) = \tilde{C}_i\hat{X}_i(j|k) \end{cases} \tag{29}$$

where $\hat{X}_i(0|k) = X_i^*(1|k-1)$.

In (27),

(i) $\left\|X_i(j|k) - X_{i,des}(j|k)\right\|_{Q_i}$ is the penalty between the predicted and its desired references, which guarantees the following vehicles in the platoon converge to the desired reference.

(ii) $\left\|\tilde{y}_i(j|k) - \hat{\tilde{y}}_i(j|k)\right\|_{G_i}$ is the penalty of the error of the trajectory of the ith vehicle and its assumed output trajectory. Minimization of $\left\|\tilde{y}_i(j|k) - \hat{\tilde{y}}_i(j|k)\right\|_{G_i}$ can avoid too much error between the assumed output trajectory $\hat{\tilde{y}}_i$ and the predicted output trajectory $\tilde{y}_i$.

(iii) $\left\|\tilde{y}_i(j|k) - \hat{\tilde{y}}_{\tilde{j}}(j|k)\right\|_{F_i}$ is the penalty of the relative error of the ith vehicle and its neighborhood. Minimization of $\left\|\tilde{y}_i(j|k) - \hat{\tilde{y}}_{\tilde{j}}(j|k)\right\|_{F_i}$ can further guarantee that the vehicle in the platoon reaches a formation.

In order to find a suitable terminal control gain K_i and a terminal penalty matrix P_i, the following Discrete Algebraic Riccati Inequality is required to be satisfied [62], [63]:

$$\left(A_i^k\right)^T P_i\left(A_i^k\right) - P_i \le -Q_i^* - K_i^T R_i K_i \tag{30}$$

where $Q_i^* = Q_i + 2|\mathbb{N}_i|(\tilde{C}_i^T F_i \tilde{C}_i)$; $|\mathbb{N}_i|$ is defined as the cardinality of set $\mathbb{N}_i$.

Further, using Schur Complement, (30) can be transformed into a linear matrix inequality (LMI) problem [60], [64]:

$$\begin{aligned} &\underset{Y_i,\,S_i}{maximize}\quad trace(Y_i) \\ &s.t\ Y_i \ge 0 \\ &\begin{bmatrix} Y_i & (A_i(v_i^x(k))Y_i + B_iS_i)^T & Y_i & S_i^T \\ A_i(v_i^x(k))Y_i + B_iS_i & Y_i & 0 & 0 \\ Y_i & 0 & Q_i^{*-1} & 0 \\ S_i & 0 & 0 & R_i^{-1} \end{bmatrix} \\ &\ge 0 \end{aligned} \tag{31}$$

with $Y_i = Y_i^T > 0$, $A_i(v_i^x(k)) \in \Omega_i$.

Thus, the terminal control gain $K_i = S_iY_i^{-1}$ and the terminal penalty matrix $P_i = Y_i^{-1}$ is computed by solving the LMI problem (31).

Furthermore, in order to find the terminal set $\mathbb{X}_i^f$, the following problem is considered [64]:

$$\begin{aligned} &\underset{Z_i}{maximize} \quad trace\,(Z_i) \\ &s.t \;\; Z_i \geq 0 \\ &\quad \begin{bmatrix} -Z_i & Z_i(A_i(v_i^x(k)) + B_i K_i)^T \\ (A_i(v_i^x(k)) + B_i K_i) Z_i & -Z_i \end{bmatrix} \\ &\quad \leq 0 \\ &\quad K_i Z_i K_i^T - \bar{u}_i^2 \leq 0 \end{aligned} \tag{32}$$

where $\bar{u}_i$ refers to the pointwise maximum of the control input. Thus, the terminal set

$$\mathbb{X}_i^f := \left\{\eta \in \mathbb{R}^n | \eta^T W_i \eta \leq 1\right\} \tag{33}$$

with $W_i = Z_i^{-1}$ is obtained by solving problem (32). Also, the terminal set $\mathbb{X}_i^f$ is a sub-level set of the terminal cost $\eta^T P_i \eta$, see [62] and [64].

Suppose Assumption 1 holds. Then, while Problem 1 is feasible at the initial time instant, the feasibility of Problem 1 can be guaranteed with the terminal penalty matrix P_i and terminal set $\mathbb{X}_i^f$, see [65] and [66].

Remark 6: Since the feasibility of Problem 1 can be guaranteed with the terminal penalty matrix P_i and terminal set $\mathbb{X}_i^f$ if Assumption 1 holds and Problem 1 is feasible at the initial time instant, the collision avoidance constraint (26i) and the road boundary constraint (26j), (26k) can be satisfied at each time instant k. That is, the safety of the vehicle platoon can be guaranteed.

Remark 7: While robust MPC can deal with uncertainties and disturbances, it is typically conservative or computationally intensive. Instead, since the inherent robustness properties of MPC with guaranteed nominal asymptotic consensus [66], [67], parameter uncertainties or disturbances of vehicle platoons need not take into account explicitly to some extent.

Remark 8: Note that the proposed scheme is suitable for various communication topologies, while different objective function is defined accordingly. Furthermore, the terminal control gain K_i, the terminal penalty matrix P_i, and the terminal set $\mathbb{X}_i^f$ need to be recomputed while different communication topologies are considered.

Remark 9: A trajectory tracking problem rather than a regulation problem is studied in this paper, which takes into account the coupled longitudinal and lateral dynamics. Thus, it has to linearise the systems along the desired trajectory if local linearization method is adopted, which might increase computational burden accordingly [68].

Remark 10: For the proposed synchronous DMPC algorithm, each vehicle does not know the predicted trajectory of other vehicles. Thus, the assumed predicted trajectory is to replace the predicted trajectory in the local optimization problems.

Remark 11: In the longitudinal direction, the control objective is to track the longitudinal velocity of the leader vehicle, and to force the inter-vehicle spacing errors converge to zero. Since each vehicle needs to transmit its assumed output trajectory to communication vehicles, and to receive the assumed output trajectory from its neighbors, the penalty terms $\left\|\tilde{y}_i(j|k) - \hat{\tilde{y}}_i(j|k)\right\|_{G_i}$ and $\left\|\tilde{y}_i(j|k) - \hat{\tilde{y}}_{\tilde{j}}(j|k)\right\|_{F_i}$ are introduced. While in the lateral direction, the control objective is to maintain the vehicle in the platoon within the designated lane, i.e., each vehicle follows the reference path.

Algorithm 1 Synchronous DMPC algorithm

Input: DMPC parameters N_p, T_s, Q_i, G_i, F_i, P_i, W_i and R_i, initial value of the state variable $X_i(0)$, control input $U_i(0)$.

Output: optimal control input $U_i^*(0|k)$.

1: Initialization. At the time instant $k = 0$, initialize the assumed control input and assumed output trajectories of the ith vehicle

$$\begin{cases} \hat{U}_i(j|k) = U_i(:|k) \\ \hat{\tilde{y}}_i(j|k) = \tilde{C}_i \hat{X}_i\,(j|k) \end{cases} \tag{34}$$

where $\hat{X}_i\,(j|k)$ is constructed as

$$\begin{aligned} &\hat{X}_i(j+1|k) \\ &= A_i\left(v_i^x(k)\right)\hat{X}_i(j|k) + B_i\hat{U}_i(j|k) + E_i w_i(j|k) \end{aligned} \tag{35}$$

with $j = 0, \cdots N_p - 1$, $\hat{X}_i\,(0|k) = X_i(0)$.

2: Iteration of DMPC. At each time instant $k \geq 0$, the following vehicles solve Problem 1 by ADMM algorithm [70] to yield the optimal control input trajectory $U_i^*(j\,|k)$.

3: Considering the assumed control sequence (28), the corresponding assumed output trajectory $\hat{\tilde{y}}_i\,(j|k+1)$ is calculated by (29).

4: Transmit the assumed output trajectory $\hat{\tilde{y}}_i\,(j|k+1)$ to communication vehicles, and receive the assumed output trajectory $\hat{\tilde{y}}_{\tilde{j}}\,(j|k+1)$ from neighbor vehicles.

5: Apply the first element of the optimal control input $U_i^*(j\,|k)$ to vehicle i.

6: At the next time instant, set $k = k+1$, and go to Step 2.

Remark 12: In order to reduce computational burden, here v_i^x in matrix $A_i\left(v_i^x(k)\right)$, $i \in [1,\ N]$ is treated as a constant parameter in the process of dynamic prediction. That is, $v_i^x\,(j|k) = v_i^x\,(0|k)$ for all $j \in \left[1,\ N_p - 1\right]$.

Remark 13: In [69], a parallel augmented Lagrange based bilinear MPC solver via a splitting scheme is proposed, which can convert the non-convex model predictive control problem into a set parallelization multi-parametric quadratic programming and an equality constrained quadratic programming problem. Thus, it can run an model predictive controller in real-time as well.

Remark 14: Proof on the string stability of vehicle platoons can be found while decoupled longitudinal and lateral controllers are designed. However, it was shown in [11] and [12] that a simply decoupled longitudinal and lateral controllers might cause a serious handling stability problem. Theoretic discussion on the aforementioned issue is still very challenging since high-order, nonlinear and coupled longitudinal and lateral dynamics are considered in this paper.

In the paper, the nonlinear model (4) of the vehicle is approximated into a linear model (15) by the Koopman operator theory. Due to the terminal quadratic constraint,

converting Problem 1 into a quadratic programming problem is difficult. A sparse solver based on the alternating direction method of multipliers (ADMM) algorithm for a linear MPC subject to the terminal quadratic constraint is adopted to solve Problem 1 [70].

The synchronous distributed model predictive control algorithm is summarized, cf. Algorithm 1.

A sufficiency condition that guarantees asymptotic consensus of the vehicle platoon with Algorithm 1 is introduced as follows.

Theorem 1 (Asymptotic Consensus of Vehicle Platoons): Suppose Assumption 1 holds. Then, asymptotic consensus of the vehicle platoon with Algorithm 1 can be guaranteed provided that

$$G_i \geq \sum_{\tilde{j}\in\Theta_i} F_{\tilde{j}}, \quad i \in N \tag{36}$$

Proof: At the time instant k, define the sum of objective function as a candidate Lyapunov function, i.e.,

$$\begin{aligned}
&J_\Sigma^*(k)\\
&=\sum_{i=1}^{N} J_i^*\big(X_i^*(:|k), U_i^*(:|k), \tilde{y}_i^*(:|k), \hat{\tilde{y}}_i(:|k), \hat{\tilde{y}}_{\tilde{j}}(:|k)\big)\\
&=\sum_{i=1}^{N}\Big\{\sum_{j=0}^{N_p-1}\big[\|X_i^*(j|k)-X_{i,des}(j|k)\|_{Q_i}+\|\tilde{y}_i^*(j|k)-\hat{\tilde{y}}_i(j|k)\|_{G_i}\\
&\qquad+\sum_{\tilde{j}\in\mathbb{N}_i}\|\tilde{y}_i^*(j|k)-\hat{\tilde{y}}_{\tilde{j}}(j|k)\|_{F_i}+\|U_i^*(j|k)\|_{R_i}\big]\\
&\qquad+\|X_i^*(N_p|k)-X_{i,des}(N_p|k)\|_{P_i}\Big\}
\end{aligned} \tag{37}$$

At the time instant $k+1$, since $\hat{U}_i(:|k+1)$ is a feasible, but not optimal control sequence, one obtains

$$\begin{aligned}
&J_\Sigma^*(k+1)-J_\Sigma^*(k)\\
&\leq\sum_{i=1}^{N} J_i\big(\hat{X}_i(:|k+1), \hat{U}_i(:|k+1), \hat{\tilde{y}}_i(:|k+1),\\
&\qquad\hat{\tilde{y}}_i(:|k+1), \hat{\tilde{y}}_{\tilde{j}}(:|k+1)\big)-J_\Sigma^*(k)\\
&\leq\sum_{i=1}^{N}\Big\{\sum_{j=0}^{N_p-1}\big[\|\hat{X}_i(j|k+1)-X_{i,des}(j|k+1)\|_{Q_i}\\
&\quad+\|\hat{\tilde{y}}_i(j|k+1)-\hat{\tilde{y}}_i(j|k+1)\|_{G_i}\\
&\quad+\sum_{\tilde{j}\in\mathbb{N}_i}\|\hat{\tilde{y}}_i(j|k+1)-\hat{\tilde{y}}_{\tilde{j}}(j|k+1)\|_{F_i}+\|\hat{U}_i(j|k+1)\|_{R_i}\big]\\
&\quad+\|\hat{X}_i(N_p|k+1)-X_{i,des}(N_p|k+1)\|_{P_i}\Big\}-J_\Sigma^*(k)
\end{aligned} \tag{38}$$

According to (28) and (29), one has

$$\begin{aligned}
&J_\Sigma^*(k+1)-J_\Sigma^*(k)\\
&\leq-\sum_{i=1}^{N}\Big\{\|X_i^*(0|k)-X_{i,des}(0|k)\|_{Q_i}+\|\tilde{y}_i^*(0|k)-\hat{\tilde{y}}_i(0|k)\|_{G_i}\\
&\qquad+\sum_{\tilde{j}\in\mathbb{N}_i}\|\tilde{y}_i^*(0|k)-\hat{\tilde{y}}_{\tilde{j}}(0|k)\|_{F_i}+\|U_i^*(0|k)\|_{R_i}\Big\}\\
&\quad+\sum_{i=1}^{N}\Delta_i+\sum_{i=1}^{N}\varepsilon_i
\end{aligned} \tag{39}$$

where

$$\begin{aligned}
\sum_{i=1}^{N}\Delta_i=\sum_{i=1}^{N}\Big\{&\sum_{j=1}^{N_p-1}\Big[\sum_{\tilde{j}\in\mathbb{N}_i}\|\tilde{y}_i^*(j|k)-\tilde{y}_{\tilde{j}}^*(j|k)\|_{F_i}\\
&-\sum_{\tilde{j}\in\mathbb{N}_i}\|\tilde{y}_i^*(j|k)-\hat{\tilde{y}}_{\tilde{j}}(j|k)\|_{F_i}\\
&-\|\tilde{y}_i^*(j|k)-\hat{\tilde{y}}_i(j|k)\|_{G_i}\Big]\Big\}
\end{aligned}$$

and

$$\begin{aligned}
\sum_{i=1}^{N}\varepsilon_i=\sum_{i=1}^{N}\Big\{&\|\hat{X}_i(N_p|k+1)-X_{i,des}(N_p|k+1)\|_{P_i}\\
&-\|X_i^*(N_p|k)-X_{i,des}(N_p|k)\|_{P_i}\\
&+\|\hat{X}_i(N_p-1|k+1)-X_{i,des}(N_p-1|k+1)\|_{Q_i}\\
&+\|K_i(\hat{X}_i(N_p-1|k+1)-X_{i,des}(N_p-1|k+1))\|_{R_i}\\
&+\sum_{\tilde{j}\in\mathbb{N}_i}\|\hat{\tilde{y}}_i(N_p-1|k+1)-\hat{\tilde{y}}_{\tilde{j}}(N_p-1|k+1)\|_{F_i}\Big\}
\end{aligned}$$

Due to the triangle inequality,

$$\begin{aligned}
\sum_{i=1}^{N}\Delta_i\leq\sum_{i=1}^{N}\Big\{&\sum_{j=1}^{N_p-1}\Big[\sum_{\tilde{j}\in\mathbb{N}_i}\|\tilde{y}_{\tilde{j}}^*(j|k)-\hat{\tilde{y}}_{\tilde{j}}(j|k)\|_{F_i}\\
&-\|\tilde{y}_i^*(j|k)-\hat{\tilde{y}}_i(j|k)\|_{G_i}\Big]\Big\}
\end{aligned} \tag{40}$$

Further, in terms of the definition of the set $\mathbb{N}_i$ and the set Θ_i, one has

$$\begin{aligned}
\sum_{i=1}^{N}\Delta_i\leq\sum_{i=1}^{N}\Big\{&\sum_{j=1}^{N_p-1}\Big[\sum_{\tilde{j}\in\Theta_i}\|\tilde{y}_i^*(j|k)-\hat{\tilde{y}}_i(j|k)\|_{F_{\tilde{j}}}\\
&-\|\tilde{y}_i^*(j|k)-\hat{\tilde{y}}_i(j|k)\|_{G_i}\Big]\Big\}
\end{aligned} \tag{41}$$

According to (36),

$$\sum_{i=1}^{N}\Delta_i\leq 0 \tag{42}$$

Similarly, due to the triangle inequality,

$$\begin{aligned}
&\sum_{i=1}^{N}\varepsilon_i\\
&\leq\sum_{i=1}^{N}\Big\{\|\hat{X}_i(N_p|k+1)-X_{i,des}(N_p|k+1)\|_{P_i}\\
&\quad-\|X_i^*(N_p|k)-X_{i,des}(N_p|k)\|_{P_i}\\
&\quad+\|\hat{X}_i(N_p-1|k+1)-X_{i,des}(N_p-1|k+1)\|_{Q_i}\\
&\quad+\|K_i(\hat{X}_i(N_p-1|k+1)-X_{i,des}(N_p-1|k+1))\|_{R_i}\\
&\quad+\sum_{\tilde{j}\in\mathbb{N}_i}\Big(\|\tilde{C}_i\hat{X}_i(N_p-1|k+1)-\tilde{C}_iX_{i,des}(N_p-1|k+1)\|_{F_i}\\
&\quad+\|\tilde{C}_i\hat{X}_{\tilde{j}}(N_p-1|k+1)-\tilde{C}_iX_{\tilde{j},des}(N_p-1|k+1)\|_{F_i}\Big)\Big\}
\end{aligned} \tag{43}$$

In terms of

$$\begin{aligned}&\left(\hat{X}_i(N_p-1|k+1)-X_{i,des}(N_p-1|k+1)\right)\\&=\left(X_i^*(N_p|k)-X_{i,des}(N_p|k)\right)\in\mathbb{X}_i^f\end{aligned}\tag{44}$$

one has

$$\begin{aligned}&\sum_{i=1}^{N}\varepsilon_i\\&\le\sum_{i=1}^{N}\Big\{\|\hat{X}_i(N_p|k+1)-X_{i,des}(N_p|k+1)\|_{P_i}\\&\quad-\|X_i^*(N_p|k)-X_{i,des}(N_p|k)\|_{P_i}\\&\quad+\|\hat{X}_i(N_p-1|k+1)-X_{i,des}(N_p-1|k+1)\|_{Q_i}\\&\quad+2|\mathbb{N}_i|\big(\|\tilde{C}_i(\hat{X}_i(N_p-1|k+1)-X_{i,des}(N_p-1|k+1))\|_{F_i}\\&\quad+\|K_i(\hat{X}_i(N_p-1|k+1)-X_{i,des}(N_p-1|k+1))\|_{R_i}\big)\Big\}\\&\le\sum_{i=1}^{N}\Big\{\|\hat{X}_i(N_p|k+1)-X_{i,des}(N_p|k+1)\|_{P_i}\\&\quad-\|X_i^*(N_p|k)-X_{i,des}(N_p|k)\|_{P_i}\\&\quad+\|\hat{X}_i(N_p-1|k+1)-X_{i,des}(N_p-1|k+1)\|_{Q_i+2|\mathbb{N}_i|(\tilde{C}_i^TF_i\tilde{C}_i)}\\&\quad+\|\hat{X}_i(N_p-1|k+1)-X_{i,des}(N_p-1|k+1)\|_{K_i^TR_iK_i}\Big\}\end{aligned}\tag{45}$$

Furthermore, in terms of (30) and (32), for any $X_{i,e}(k)\in\mathbb{X}_i^f$ and $k>0$, the terminal control law $U_i(k)=K_iX_{i,e}(k)$ and the terminal cost $V_i(X_{i,e}(k))=X_{i,e}(k)^TP_iX_{i,e}(k)$ satisfies

$$\begin{aligned}&V_i\left(\hat{X}_{i,e}(N_p|k+1)\right)-V_i\left(X_{i,e}^*(N_p|k)\right)\\&\qquad\le-\|X_{i,e}^*(N_p|k)\|_{Q_i^*}-\|X_{i,e}^*(N_p|k)\|_{K_i^TR_iK_i}\end{aligned}\tag{46}$$

Combining (45) and (46), then

$$\sum_{i=1}^{N}\varepsilon_i\le 0\tag{47}$$

Substituting both (42) and (47) into (39), one can conclude

$$\begin{aligned}&J_\Sigma^*(k+1)-J_\Sigma^*(k)\\&\le-\sum_{i=1}^{N}\Big\{\|X_i^*(0|k)-X_{i,des}(0|k)\|_{Q_i}+\|\tilde{y}_i^*(0|k)-\hat{\tilde{y}}_i(0|k)\|_{G_i}\\&\qquad+\sum_{\tilde{j}\in\mathbb{N}_i}\|\tilde{y}_i^*(0|k)-\hat{\tilde{y}}_{\tilde{j}}(0|k)\|_{F_i}+\|U_i^*(0|k)\|_{R_i}\Big\}\\&\le 0.\end{aligned}\tag{48}$$

This means that $J_\Sigma^*(k)$ is monotonically decreasing. Accordingly, the state of each vehicle in the platoon will converge to the reference trajectory, i.e., $\lim_{k\to\infty}X_{i,e}(k)=0$, and $\lim_{k\to\infty}v_i^x(k)=v_0^x(k)$, $i\in 1,\ldots,N$. Therefore, asymptotic consensus of vehicle platoons is guaranteed.

B. Lower-Level Controller

The steering angle of the front tire calculated by the distributed model predictive controller can be directly transformed into steering wheel angle by a vehicle's steering ratio [37]. However, the desired longitudinal control force cannot be implemented directly on a real vehicle. Therefore, a lower-level controller is designed to transform the desired longitudinal control force into throttle angle and brake pressure by an inverse longitudinal dynamics model of the vehicle [71], [73]. The structure of the lower-level controller is shown in Fig. 8.

1) In the Process of Driving (When F_i^x Is the Driving Force): The driving force is provided by the engine of the vehicle, so the desired engine torque can be calculated [71], i.e.,

$$T_{des,i}=\frac{F_i^x\,r_{eff,i}}{i_{g,i}\,i_{o,i}\,\eta_{T,i}}\tag{49}$$

The engine torque characteristic map is shown in Fig. 9. Utilizing the desired engine torque $T_{des,i}$ and the current engine speed $w_{e,i}$, the desired throttle angle $\alpha_{des,i}$ is obtained [72], where

$$\alpha_{des,i}=\beta_i^{-1}\left(T_{des,i},w_{e,i}\right)\tag{50}$$

and the term $\beta_i^{-1}:(T_{des,i})\times(w_{e,i})\to(\alpha_{des,i})$ represents a mapping.

2) In the Process of Braking (When F_i^x Is the Braking Force): The desired braking force and braking pressure satisfy a linear relationship [73], i.e.,

$$p_{bdes,i}=\frac{F_i^x}{K_s}\tag{51}$$

where K_s is the braking coefficient,

$$K_s=\frac{T_{bf,i}-T_{br,i}}{p_{b,i}\,r_{eff,i}}\tag{52}$$

the term $p_{b,i}$ is the braking pressure, $T_{bf,i}$ and $T_{br,i}$ are the braking torques of the front and rear wheels, respectively.

IV. Simulation and Result Analysis

A vehicle platoon consists of five vehicles, namely, one leader vehicle and four followers. A joint simulation platform consisting of PreScan, CarSim, and Matlab/Simulink is constructed, which is shown in Fig. 10, where Prescan provides the road environment information, CarSim provides the vehicle dynamics, and Matlab/Simulink is employed to design and implement of controller. All vehicle parameters in the joint simulation are the same except for the vehicle mass m_i, i.e., $I_i^z=I^z$, $a_i=a$, $b_i=b$, $C_i^{cf}=C^{cf}$, $C_i^{cr}=C^{cr}$, $\eta_{T,i}=\eta_T$, $r_{eff,i}=r_{eff}$, $i_{g,i}=i_g$, $i_{o,i}=i_o$. Set $m_0=1820\,\text{kg}$, $m_1=1845\,\text{kg}$, $m_2=1868\,\text{kg}$, $m_3=1922\,\text{kg}$, $m_4=1984\,\text{kg}$. The parameters of the vehicle dynamics are shown in Table I.

The braking coefficient of K_s is produced as follows: set the initial velocity of the vehicle in CarSim to 70km/h, and the braking pressure of $P_{b,i}=0.8$Mpa, then the braking torque of the front wheels $T_{bf,i}=320\text{N}\cdot\text{m}$, and the braking torque of the rear wheels $T_{br,i}=320\text{N}\cdot\text{m}$ are measured, respectively. According to (52), $K_s=2266.3$.

The following parameters and constraints are used in the design of DMPC, i.e.,

- Sampling time: $T_s=0.1$s
- Prediction horizon: $N_p=6$

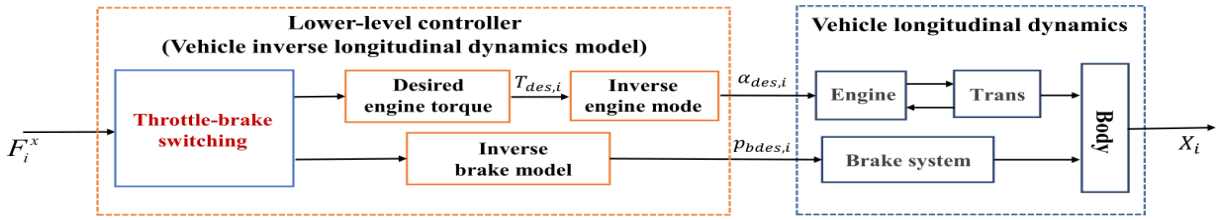

Fig. 8. The structure of the lower-level controller.

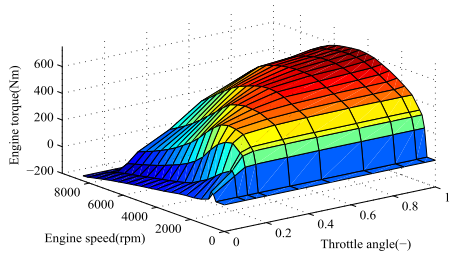

Fig. 9. Engine torque map.

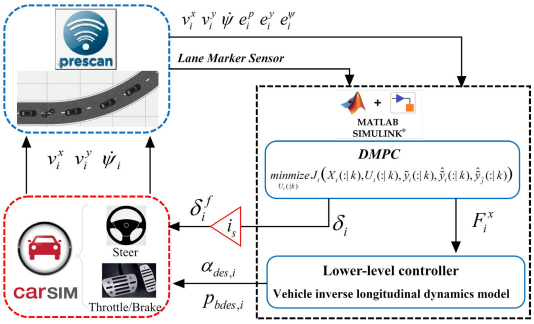

Fig. 10. The structure of the joint simulation by PreScan, CarSim, and Simulink.

TABLE I

THE PARAMETERS OF THE VEHICLE DYNAMICS

Parameters	Value	Parameters	Value
i_s	18.03	C^{cf}	81473(N/rad)
I^z	4095(kg · m^2)	C^{cr}	62469(N/rad)
a	1.265(m)	r_{eff}	0.353(m)
b	1.675(m)	i_o	2.65
η_T	0.99	i_g	[4.595, 2.724, 1.864, 1.464, 1.231, 1.0, 0.824, 0.685]

- State constraints [74]:
  $v^x_{i,min} = 10$(m/s), $v^x_{i,max} = 30$(m/s)
  $v^y_{i,min} = -2$(m/s), $v^y_{i,max} = 2$(m/s)
  $\dot{\psi}_{i,min} = -0.2$(rad/s), $\dot{\psi}_{i,max} = 0.2$(rad/s)
  $e^p_{i,min} = -2$(m), $e^p_{i,max} = 2$(m)
  $e^\psi_{i,min} = -0.1$(rad), $e^\psi_{i,max} = 0.1$(rad)
  $e^y_{i,min} = -1$(m), $e^y_{i,max} = 1$(m)
- Actuator constraints [37]:
  $F^x_{i,min} = -5000$(N), $F^x_{i,max} = 5000$(N)
  $\delta_{i,min} = -0.7$(rad), $\delta_{i,max} = 0.7$(rad).

Set the initial position of the leader vehicle as $s_0 = 64$m, the initial positions of the following vehicles as $s_1 = 48$m, $s_2 = 32$m, $s_3 = 16$m, $s_4 = 0$m, respectively. A constant distance policy is adopted, i.e., $d_0 = 16$m (when $v^x_0 = 20$m/s, constant time headway is 0.8s). The desired velocity trajectory of the leader vehicle is shown in Fig. 11, i.e., the leader vehicle in the platoon is running along a given curved road. The road radius is shown in Fig. 12.

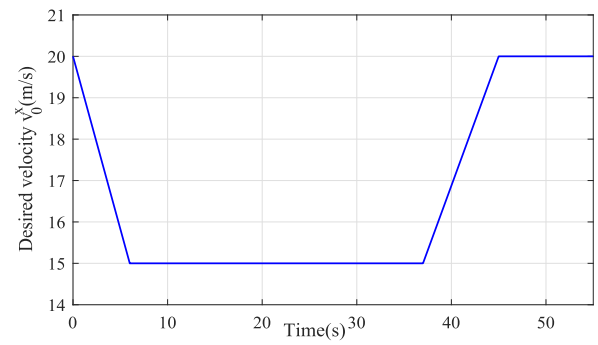

Fig. 11. The desired velocity trajectory of the leader vehicle.

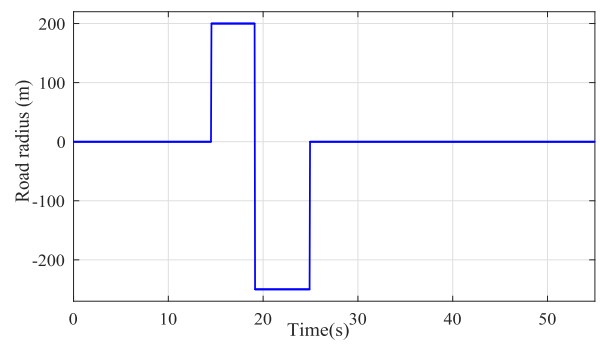

Fig. 12. The road radius.

Remark 15: Note that for comparison, a DMPC algorithm solving directly a nonlinear optimization problem without the terminal constraint is designed, where the nonlinear vehicle dynamics model (4) and the lane-keeping model (18) are taken into account directly.

Case 1: Vehicle Platoon Under the Predecessor-Leader Following Communication Topology: In the joint simulation, first, a vehicle platoon with five vehicles interconnected by the predecessor-leader following (PLF) communication topology is considered, which is shown in Fig. 13, where each following vehicle of the platoon can obtain the information of its predecessor vehicle and leader vehicle simultaneously.

The joint simulation results under the PLF communication topology are shown in Fig. 14-21. Fig. 14 shows the longitudinal position of the vehicle in the platoon when the leader vehicle velocity changes, where the collision can be avoided.

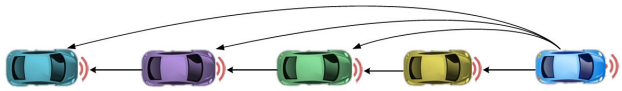

Fig. 13. The predecessor-leader following communication topology.

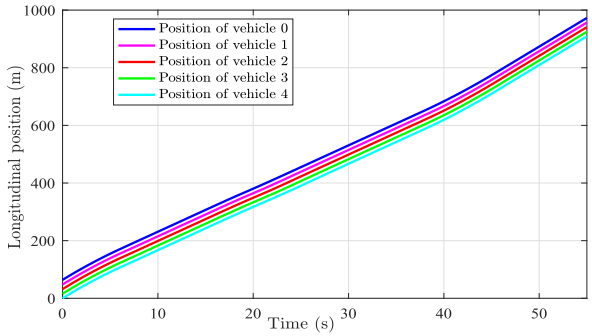

Fig. 14. Longitudinal position of the vehicle under the PLF communication topology.

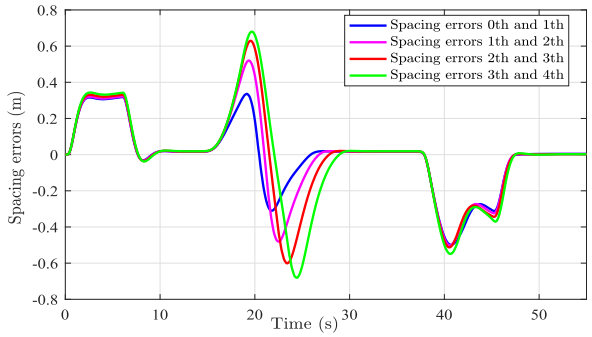

Fig. 15. Spacing errors of the following vehicles under the PLF communication topology.

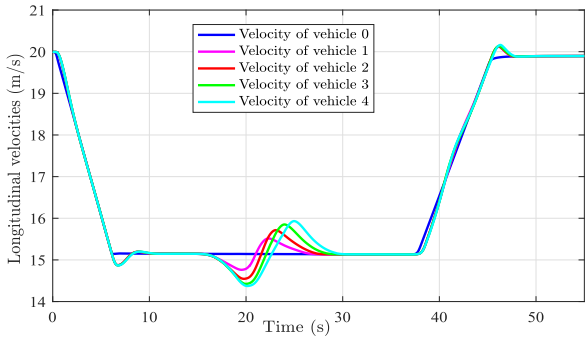

Fig. 16. Longitudinal velocity of the following vehicles under the PLF communication topology.

Fig. 15 shows spacing errors of the following vehicles in the platoon, where the desired safety distance can be maintained between the front and rear vehicles. Fig. 16 shows that when the leader vehicle changes its velocity, the following vehicles in the platoon can track the velocity of the leader vehicle. Fig. 17-18 show the performance of lane keeping for vehicle in the platoon when the leader vehicle velocity changes. It can be found that when the road curvature changes, the lateral position error and heading error of vehicles in the platoon will change accordingly within an allowable range. When the road curvature is constant, the lateral state information of

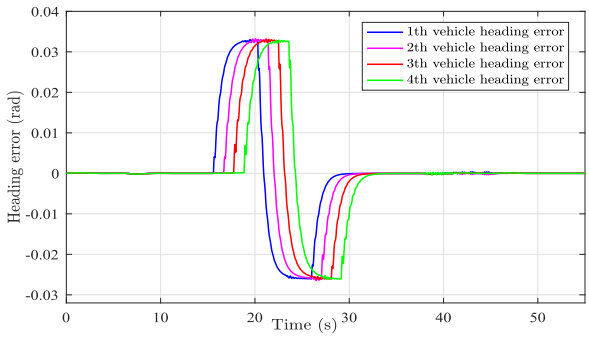

Fig. 17. Heading error of the following vehicles under the PLF communication topology.

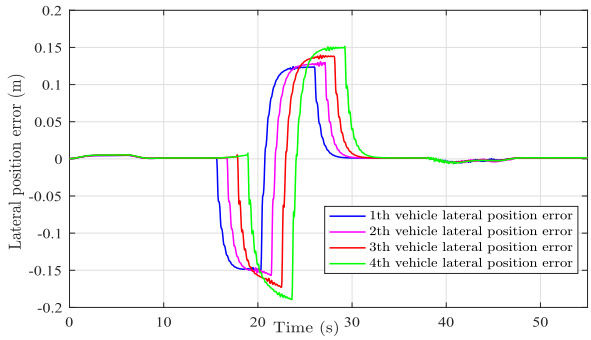

Fig. 18. Lateral position error of the following vehicles under the PLF communication topology.

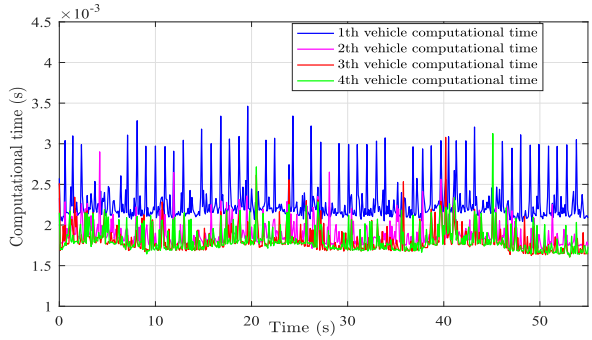

Fig. 19. Computational time of the proposed algorithm with the terminal constraint under the PLF communication topology.

vehicles will converge to zero. The computational time of the proposed algorithm with the terminal constraint under the PLF communication topology is shown in Fig. 19, which operated on Intel(R) Core(TM) i7-10700 CPU(2.90GHz), and 16GB RAM. The average computational time of the four following vehicles is 0.0023s, 0.0019s, 0.0018s, 0.0018s, respectively. As a comparison, the computational time for solving the nonlinear optimization problem without the terminal constraint using the MATLAB function 'fmincon' (MATLAB 2016b, active-set method) under the PLF communication topology is shown in Fig. 20. The average computational time of the four following vehicles is 0.1197s, 0.1257s, 0.1235s, 0.1264s, respectively. The computational time for solving the nonlinear optimization problem without the terminal constraint using ACADO Code Generation tool under the PLF communication topology is shown in Fig. 21. The average computational time of the four following vehicles is 4.537×10^{-5}s, 4.544×10^{-5}s,

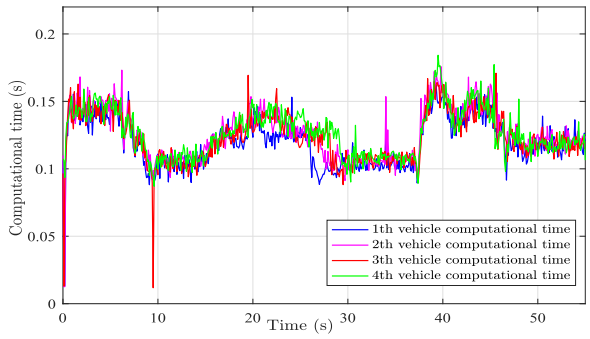

Fig. 20. Computational time for solving the nonlinear optimization problem without the terminal constraint using the MATLAB function 'fmincon' (active-set method) under the PLF communication topology.

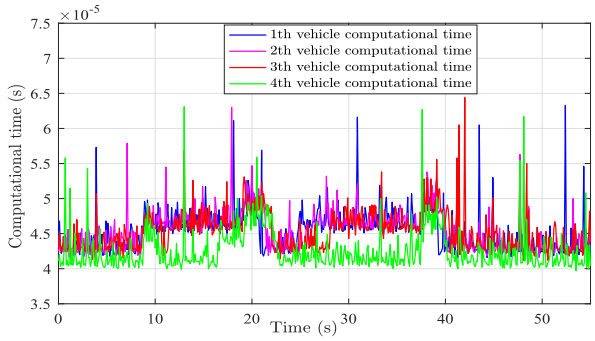

Fig. 21. Computational time for solving the nonlinear optimization problem without the terminal constraint using ACADO Code Generation tool under the PLF communication topology.

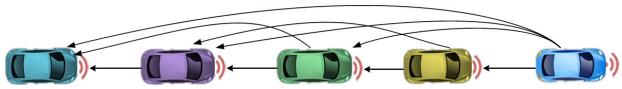

Fig. 22. The two-predecessor-leader following communication topology.

4.531×10^{-5}s, 4.263×10^{-5}s, respectively. Although the nonlinear optimization problem can be solved directly using the ACADO Code Generation tool with less computational time, the asymptotic consensus might not be guaranteed due to the lack of a terminal constraint. Compared to solving nonlinear optimization problems using the MATLAB function 'fmincon', the proposed algorithm can significantly reduce the computational burden.

Case 2: Vehicle Platoon Under the Two-Predecessor-Leader Following Communication Topology: Here a vehicle platoon under the two-predecessor-leader following (TPLF) communication topology shown in Fig. 22 is considered, where the following vehicles in the platoon can obtain the information of its two predecessor vehicles and leader vehicle simultaneously.

The joint simulation results under the TPLF communication topology are shown in Fig. 23-29. Fig. 23-25 shows that when the leader vehicle changes its velocity, the following vehicles in the platoon can still quickly converge to the velocity of the leader vehicle, and maintain the desired safety distance. It can be found in Fig. 26-27 that the vehicles in the platoon can still keep in the lane under the TPLF communication topology. The computational time of the proposed algorithm with the terminal constraint under the TPLF communication topology is shown in Fig. 28, which operated on Intel(R) Core(TM) i7-10700 CPU(2.90GHz), and 16GB RAM. The average computational time of the four following vehicles

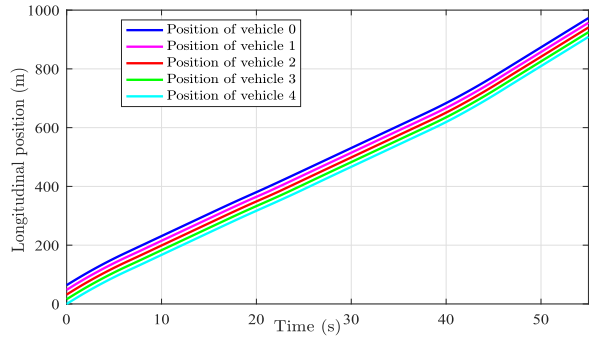

Fig. 23. Longitudinal position of the vehicle under the TPLF communication topology.

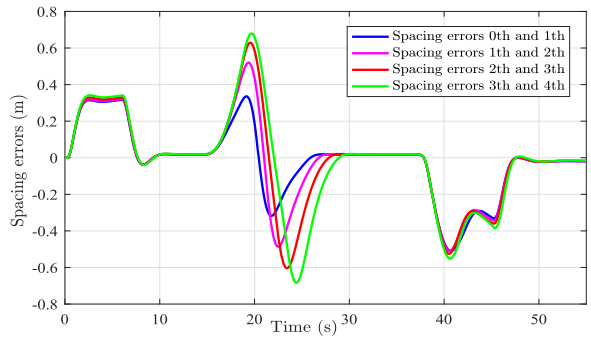

Fig. 24. Spacing errors of the following vehicles under the TPLF communication topology.

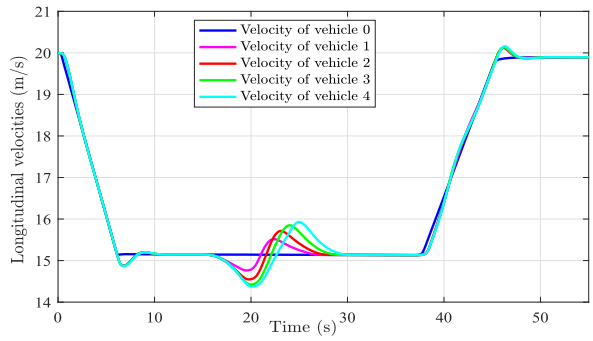

Fig. 25. Longitudinal velocity of the following vehicles under the TPLF communication topology.

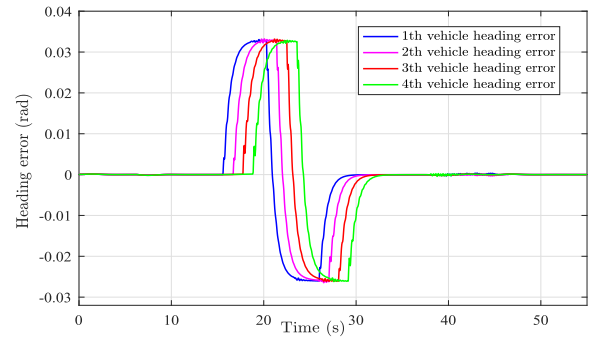

Fig. 26. Heading error of the following vehicles under the TPLF communication topology.

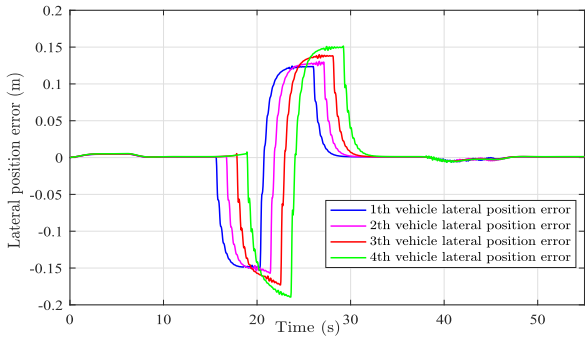

Fig. 27. Lateral position error of the following vehicles under the TPLF communication topology.

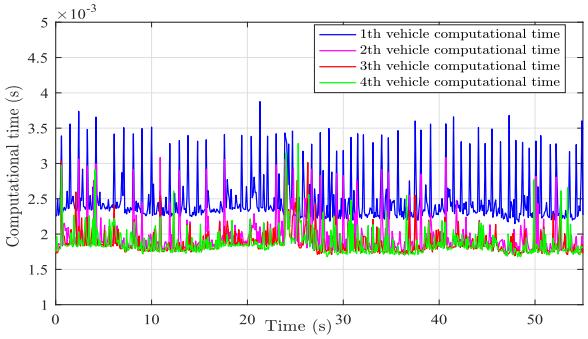

Fig. 28. Computational time of the proposed algorithm with the terminal constraint under the TPLF communication topology.

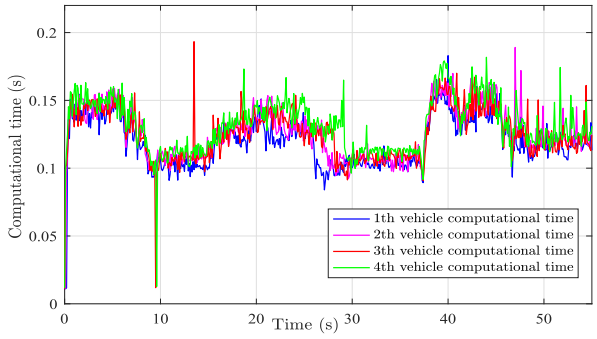

Fig. 29. Computational time for solving the nonlinear optimization problem without the terminal constraint using the MATLAB function 'fmincon' (active-set method) under the TPLF communication topology.

is 0.0025s, 0.0020s, 0.0019s, 0.0019s, respectively. As a comparison, the computational time for solving the nonlinear optimization problem without the terminal constraint using the MATLAB function 'fmincon' (MATLAB 2016b, active-set method) under the TPLF communication topology is shown in Fig. 29. The average computational time of the four following vehicles is 0.1195s, 0.1257s, 0.1254s, 0.1314s, respectively. Compared to solving nonlinear optimization problems using the MATLAB function 'fmincon', the proposed algorithm can significantly reduce the computational burden.

Remark 16: In the paper, a nonlinear vehicle platoon model is approximated to a linear parametric-varying model using the Koopman operator theory. Furthermore, a linear DMPC optimization problem subject to terminal quadratic constraints is designed to guarantee asymptotic consensus, which avoids solving nonlinear optimization problems and reduces the computational burden accordingly. Note that asymptotic consensus of the vehicle platoon can be guaranteed by adding a terminal constraint into the optimization problem [23], [66]. Future research will focus on solving the linear DMPC optimization problem subject to the terminal quadratic constraint using the ACADO Code Generation tool to reduce computational time further [75].

TABLE II
COUPLED LONGITUDINAL AND LATERAL CONTROL

Weight	Value
Q_i	$10^6\text{diag}(8, 8, 8, 500, 10, 10)$
G_i	$10^6\text{diag}(1, 1, 1, 100, 1, 1)$
F_i	$10^4\text{diag}(1, 1, 1, 100, 1, 1)$
R_i	$\text{diag}(10, 10)$

V. CONCLUSION

There exists a strong coupling relationship between the longitudinal and lateral motion of a vehicle platoon driving on the curved road. In this paper, a hierarchical control structure combining longitudinal tracking and lane-keeping was presented for communication vehicles in the platoon. Firstly, a nonlinear vehicle model considering the coupling characteristics of longitudinal and lateral dynamics was approximated to a "global" linear model by the Koopman operator theory. Combining linearized vehicle dynamics model and the lane-keeping model, a linear parametric-varying vehicle platoon model was established. Then, a synchronous distributed model predictive control algorithm with the vehicle platoon model was proposed as an upper-level controller, which can reduce the computational burden accordingly. A lower-level controller was designed, where the desired longitudinal control force determined by the upper-level controller was transformed into throttle angle and brake pressure by the inverse longitudinal dynamics model of the vehicle. Finally, joint simulation results by PreScan, CarSim and MATLAB/Simulink showed that when a vehicle platoon driving on a curved road, the proposed control strategy guarantees a good performance on both longitudinal tracking and lane keeping. Future research will focus on guaranteeing the string stability of vehicle platoons, and addressing communication delays or data packet loss between vehicles.

APPENDIX

The parameters of coupled longitudinal and lateral control are listed in Table II.

Solving the LMI problem (31) and the terminal region problem (32) under the PLF communication topology, we obtain the matrices

$$K_1 = \begin{bmatrix} -3310.8 & 0.3605 & 2.7188 & -3326.7 & -3.2486 & -30.7785 \\ 0.0017 & -0.1506 & -0.7211 & 0.0013 & 0.5689 & 4.1244 \end{bmatrix}$$

$$K_2 = \begin{bmatrix} -3311.4 & 0.3422 & 2.7074 & -3306.3 & -3.2810 & -31.1075 \\ 0.0017 & -0.1533 & -0.7235 & 0.0013 & 0.5732 & 4.1687 \end{bmatrix}$$

$$K_3=\begin{bmatrix} -3309.3 & 0.2996 & 2.6821 & -3254.4 & -3.3518 & -31.8513 \\ 0.0017 & -0.1595 & -0.7292 & 0.0013 & 0.5835 & 4.2745 \end{bmatrix}$$

$$K_4=\begin{bmatrix} -3306.3 & 0.2494 & 2.6570 & -3197.2 & -3.4356 & -32.6980 \\ 0.0018 & -0.1670 & -0.7359 & 0.0013 & 0.5956 & 4.3981 \end{bmatrix}$$

$$P_1=10^6\begin{bmatrix} 689.12 & -0.0605 & -0.4804 & 817.86 & 0.6431 & 5.9092 \\ 0.0605 & 25.906 & -7.8829 & -0.0872 & -32.500 & -202.90 \\ -0.4804 & -7.8829 & 72.689 & -0.3062 & -30.998 & -211.47 \\ 817.86 & -0.0872 & -0.3062 & 2921.8 & 0.8502 & 6.6277 \\ 0.6431 & -32.500 & -30.998 & 0.8502 & 112.88 & 521.10 \\ 5.9092 & -202.90 & -211.47 & 6.6277 & 521.10 & 4451.0 \end{bmatrix}$$

$$P_2=10^6\begin{bmatrix} 697.11 & -0.0581 & -0.4838 & 822.16 & 0.6558 & 6.0336 \\ 0.0581 & 26.437 & -7.7966 & -0.0931 & -33.299 & -209.48 \\ -0.4838 & -7.7966 & 71.973 & -0.3054 & -30.829 & -210.59 \\ 822.16 & -0.0931 & -0.3054 & 2934.6 & 0.8616 & 6.7354 \\ 0.6558 & -33.299 & -30.829 & 0.8616 & 113.86 & 529.49 \\ 6.0336 & -209.48 & -210.59 & 6.7354 & 529.49 & 4531.8 \end{bmatrix}$$

$$P_3=10^6\begin{bmatrix} 715.98 & -0.0524 & -0.4921 & 830.22 & 0.6854 & 6.3262 \\ 0.0524 & 27.716 & -7.5656 & -0.1073 & -35.215 & -225.32 \\ -0.4921 & -7.5656 & 70.350 & -0.3052 & -30.503 & -208.99 \\ 830.22 & -0.1073 & -0.3052 & 2947.6 & 0.8883 & 6.9977 \\ 0.6854 & -35.215 & -30.503 & 0.8883 & 116.23 & 549.73 \\ 6.3262 & -225.32 & -208.99 & 6.9977 & 549.73 & 4726.2 \end{bmatrix}$$

$$P_4=10^6\begin{bmatrix} 735.33 & -0.0452 & -0.5021 & 839.28 & 0.7203 & 6.6668 \\ 0.0452 & 29.236 & -7.2530 & -0.1240 & -37.471 & -244.11 \\ -0.5021 & -7.2530 & 68.589 & -0.3059 & -30.245 & -207.90 \\ 839.28 & -0.1240 & -0.3059 & 2962.6 & 0.9200 & 7.2987 \\ 0.7203 & -37.471 & -30.245 & 0.9200 & 119.03 & 573.75 \\ 6.6668 & -244.11 & -207.90 & 7.2987 & 573.75 & 4995.6 \end{bmatrix}$$

$$W_1=\begin{bmatrix} 0.4406 & -0.0007 & -0.0100 & 0.4566 & 0.0039 & 0.0235 \\ -0.0007 & 0.0711 & 0.2608 & -0.0003 & -0.2749 & -1.5657 \\ -0.0100 & 0.2608 & 1.2493 & -0.0088 & -1.0099 & -6.6562 \\ 0.4566 & -0.0003 & -0.0088 & 0.5781 & 0.0028 & 0.0244 \\ 0.0039 & -0.2749 & -1.0099 & 0.0028 & 1.0690 & 6.1023 \\ 0.0235 & -1.5657 & -6.6562 & 0.0244 & 6.1023 & 41.441 \end{bmatrix}$$

$$W_2=\begin{bmatrix} 0.4405 & -0.0007 & -0.0098 & 0.4525 & 0.0039 & 0.0243 \\ -0.0007 & 0.0736 & 0.2656 & -0.0003 & -0.2817 & -1.6122 \\ -0.0098 & 0.2656 & 1.2538 & -0.0085 & -1.0184 & -6.7388 \\ 0.4525 & -0.0003 & -0.0085 & 0.5694 & 0.0027 & 0.0247 \\ 0.0039 & -0.2817 & -1.0184 & 0.0027 & 1.0850 & 6.2218 \\ 0.0243 & -1.6122 & -6.7388 & 0.0247 & 6.2218 & 42.323 \end{bmatrix}$$

$$W_3=\begin{bmatrix} 0.4394 & -0.0007 & -0.0095 & 0.4422 & 0.0039 & 0.0258 \\ -0.0007 & 0.0797 & 0.2773 & -0.0003 & -0.2984 & -1.7261 \\ -0.0095 & 0.2773 & 1.2648 & -0.0079 & -1.0390 & -6.9371 \\ 0.4422 & -0.0003 & -0.0079 & 0.5477 & 0.0026 & 0.0256 \\ 0.0039 & -0.2984 & -1.0390 & 0.0026 & 1.1239 & 6.5116 \\ 0.0258 & -1.7261 & -6.9371 & 0.0256 & 6.5116 & 44.471 \end{bmatrix}$$

$$W_4=\begin{bmatrix} 0.4381 & -0.0007 & -0.0091 & 0.4307 & 0.0039 & 0.0275 \\ -0.0007 & 0.0872 & 0.2913 & -0.0003 & -0.3187 & -1.8650 \\ -0.0091 & 0.2913 & 1.2781 & -0.0072 & -1.0635 & -7.1713 \\ 0.4307 & -0.0003 & -0.0072 & 0.5243 & 0.0026 & 0.0264 \\ 0.0039 & -0.3187 & -1.0635 & 0.0026 & 1.1708 & 6.8590 \\ 0.0275 & -1.8650 & -7.1713 & 0.0264 & 6.8590 & 47.058 \end{bmatrix}$$

The parameters of the terminal ingredients obtained by solving the LMI problem (31) and the terminal region problem (32) under the TPLF communication topology are ignored due to the space limitation.

References

[1] F. Fakhfakh, M. Tounsi, and M. Mosbah, "Vehicle platooning systems: Review, classification and validation strategies," *Int. J. Netw. Distrib. Comput.*, vol. 8, no. 4, pp. 203–213, Oct. 2020.

[2] A. Petrillo, A. Pescapé, and S. Santini, "A secure adaptive control for cooperative driving of autonomous connected vehicles in the presence of heterogeneous communication delays and cyberattacks," *IEEE Trans. Cybern.*, vol. 51, no. 3, pp. 1134–1149, Mar. 2021.

[3] S. E. Li, Y. Zheng, K. Li, and J. Wang, "An overview of vehicular platoon control under the four-component framework," in *Proc. IEEE Intell. Vehicles Symp. (IV)*, Seoul, South Korea, Jun. 2015, pp. 286–291.

[4] F. Lin, M. Fardad, and M. R. Jovanovic, "Optimal control of vehicular formations with nearest neighbor interactions," *IEEE Trans. Autom. Control*, vol. 57, no. 9, pp. 2203–2218, Sep. 2012.

[5] H. Hao and P. Barooah, "Stability and robustness of large platoons of vehicles with double-integrator models and nearest neighbor interaction," *Int. J. Robust Nonlinear Control*, vol. 23, no. 18, pp. 2097–2122, Dec. 2013.

[6] Q. Wang, G. Guo, and B. Cai, "Distributed receding horizon control for fuel-efficient and safe vehicle platooning," *Sci. China Technol. Sci.*, vol. 59, no. 12, pp. 1953–1962, Dec. 2016.

[7] Y. Zheng, S. E. Li, K. Li, F. Borrelli, and J. K. Hedrick, "Distributed model predictive control for heterogeneous vehicle platoons under unidirectional topologies," *IEEE Trans. Control Syst. Technol.*, vol. 25, no. 3, pp. 899–910, May 2017.

[8] F. Gao, X. Hu, S. E. Li, K. Li, and Q. Sun, "Distributed adaptive sliding mode control of vehicular platoon with uncertain interaction topology," *IEEE Trans. Ind. Electron.*, vol. 65, no. 8, pp. 6352–6361, Aug. 2018.

[9] D. Zhang, K. Li, and J. Wang, "A curving ACC system with coordination control of longitudinal car-following and lateral stability," *Vehicle Syst. Dyn.*, vol. 50, no. 7, pp. 1085–1102, Jul. 2012.

[10] R. Rajamani, H.-S. Tan, B. Kait Law, and W.-B. Zhang, "Demonstration of integrated longitudinal and lateral control for the operation of automated vehicles in platoons," *IEEE Trans. Control Syst. Technol.*, vol. 8, no. 4, pp. 695–708, Jul. 2000.

[11] L. Li, X. G. Yao, and S. Shi, "An analysis on the effects of tire nonlinearity on autonomous platoon stability," *Automot. Eng.*, vol. 41, no. 9, pp. 1065–1072, Sep. 2019.

[12] S. Shi, L. Li, Y. Mu, and G. Chen, "Stable headway prediction of vehicle platoon based on the 5-degree-of-freedom vehicle model," *Proc. Inst. Mech. Eng., D, J. Automobile Eng.*, vol. 233, no. 6, pp. 1570–1585, May 2019.

[13] S. G. Loizou, D. G. Lui, A. Petrillo, and S. Santini, "Connectivity preserving formation stabilization in an obstacle-cluttered environment in the presence of time-varying communication delays," *IEEE Trans. Autom. Control*, vol. 67, no. 10, pp. 5525–5532, Oct. 2022, doi: 10.1109/TAC.2021.3119003.

[14] S. E. Li et al., "Dynamical modeling and distributed control of connected and automated vehicles: Challenges and opportunities," *IEEE Intell. Transp. Syst. Mag.*, vol. 9, no. 3, pp. 46–58, Fall. 2017.

[15] A. A. Peters, R. H. Middleton, and O. Mason, "Leader tracking in homogeneous vehicle platoons with broadcast delays," *Automatica*, vol. 50, no. 1, pp. 64–74, Jan. 2014.

[16] S. E. Li, Y. Zheng, K. Li, L.-Y. Wang, and H. Zhang, "Platoon control of connected vehicles from a networked control perspective: Literature review, component modeling, and controller synthesis," *IEEE Trans. Veh. Technol.*, early access, Jul. 6, 2018, doi: 10.1109/TVT.2017.2723881.

[17] Y. Wu, S. E. Li, J. Cortés, and K. Poolla, "Distributed sliding mode control for nonlinear heterogeneous platoon systems with positive definite topologies," *IEEE Trans. Control Syst. Technol.*, vol. 28, no. 4, pp. 1272–1283, Jul. 2020.

[18] F. Gao, S. E. Li, Y. Zheng, and D. Kum, "Robust control of heterogeneous vehicular platoon with uncertain dynamics and communication delay," *IET Intell. Transp. Syst.*, vol. 10, no. 7, pp. 503–513, Sep. 2016.

[19] D. G. Lui, A. Petrillo, and S. Santini, "Leader tracking control for heterogeneous uncertain nonlinear multi-agent systems via a distributed robust adaptive PID strategy," *Nonlinear Dyn.*, vol. 108, no. 1, pp. 363–378, Mar. 2022.

[20] G. De Tommasi, D. G. Lui, A. Petrillo, and S. Santini, "A L2-gain robust PID-like protocol for time-varying output formation-containment of multi-agent systems with external disturbance and communication delays," *IET Control Theory Appl.*, vol. 15, no. 9, pp. 1169–1184, Jun. 2021.

[21] D. G. Lui, A. Petrillo, and S. Santini, "Distributed model reference adaptive containment control of heterogeneous multi-agent systems with unknown uncertainties and directed topologies," *J. Franklin Inst.*, vol. 358, no. 1, pp. 737–756, Jan. 2021.

[22] R. R. Negenborn and J. M. Maestre, "Distributed model predictive control: An overview and roadmap of future research opportunities," *IEEE Control Syst. Mag.*, vol. 34, no. 4, pp. 87–97, Aug. 2014.

[23] P. D. Christofides, R. Scattolini, D. M. de la Peña, and J. Liu, "Distributed model predictive control: A tutorial review and future research directions," *Comput. Chem. Eng.*, vol. 51, pp. 21–41, Apr. 2013.

[24] W. B. Dunbar and D. S. Caveney, "Distributed receding horizon control of vehicle platoons: Stability and string stability," *IEEE Trans. Autom. Control*, vol. 57, no. 3, pp. 620–633, Mar. 2012.

[25] M. Yan, W. Ma, L. Zuo, and P. Yang, "Dual-mode distributed model predictive control for platooning of connected vehicles with nonlinear dynamics," *Int. J. Control, Autom. Syst.*, vol. 17, no. 12, pp. 3091–3101, Dec. 2019.

[26] S. Yu et al., "Nash optimality based distributed model predictive control for vehicle platoon," *IFAC-PapersOnLine*, vol. 53, no. 2, pp. 6610–6615, 2020.

[27] Y. Zhou, M. Wang, and S. Ahn, "Distributed model predictive control approach for cooperative car-following with guaranteed local and string stability," *Transp. Res. B, Methodol.*, vol. 128, pp. 69–86, Oct. 2019.

[28] P. Wang, H. Deng, J. Zhang, L. Wang, M. Zhang, and Y. Li, "Model predictive control for connected vehicle platoon under switching communication topology," *IEEE Trans. Intell. Transp. Syst.*, vol. 23, no. 7, pp. 7817–7830, Jul. 2022, doi: 10.1109/TITS.2021.3073012.

[29] C. Chang and Z. Yuan, "Combined longitudinal and lateral control of vehicle platoons," in *Proc. Int. Conf. Comput. Syst., Electron. Control (ICCSEC)*, Dalian, China, Dec. 2017, pp. 848–853.

[30] L. Xu, W. Zhuang, G. Yin, G. Li, and C. Bian, "Simultaneous longitudinal and lateral control of vehicle platoon subject to stochastic communication delays," *J. Dyn. Syst., Meas., Control*, vol. 141, no. 4, Apr. 2019, Art. no. 044503.

[31] T. Fujioka and M. Omae, "Vehicle following control in lateral direction for platooning," *Vehicle Syst. Dyn.*, vol. 29, no. 1, pp. 422–437, Jan. 1998.

[32] S. Wei, Y. Zou, X. Zhang, T. Zhang, and X. Li, "An integrated longitudinal and lateral vehicle following control system with radar and vehicle-to-vehicle communication," *IEEE Trans. Veh. Technol.*, vol. 68, no. 2, pp. 1116–1127, Feb. 2019.

[33] B. Caiazzo, D. G. Lui, A. Petrillo, and S. Santini, "Distributed double-layer control for coordination of multiplatoons approaching road restriction in the presence of IoV communication delays," *IEEE Internet Things J.*, vol. 9, no. 6, pp. 4090–4109, Mar. 2022.

[34] R. Kianfar, M. Ali, P. Falcone, and J. Fredriksson, "Combined longitudinal and lateral control design for string stable vehicle platooning within a designated lane," in *Proc. 17th Int. IEEE Conf. Intell. Transp. Syst. (ITSC)*, Qingdao, China, Oct. 2014, pp. 1003–1008.

[35] J. Lan, D. Zhao, and D. Tian, "Robust cooperative adaptive cruise control of vehicles on banked and curved roads with sensor bias," in *Proc. Amer. Control Conf. (ACC)*, Denver, CO, USA, Jul. 2020, pp. 2276–2281.

[36] A. Bayuwindra, J. Ploeg, E. Lefeber, and H. Nijmeijer, "Combined longitudinal and lateral control of car-like vehicle platooning with extended look-ahead," *IEEE Trans. Control Syst. Technol.*, vol. 28, no. 3, pp. 790–803, May 2020.

[37] D. Dang, F. Gao, and Q. Hu, "Motion planning for autonomous vehicles considering longitudinal and lateral dynamics coupling," *Appl. Sci.*, vol. 10, no. 9, p. 3180, May 2020.

[38] N. Chowdhri, L. Ferranti, F. S. Iribarren, and B. Shyrokau, "Integrated nonlinear model predictive control for automated driving," *Control Eng. Pract.*, vol. 106, Jan. 2021, Art. no. 104654.

[39] H. Zhao, X. Lu, H. Chen, Q. Liu, and B. Gao, "Coordinated attitude control of longitudinal, lateral and vertical tyre forces for electric vehicles based on model predictive control," *IEEE Trans. Veh. Technol.*, vol. 71, no. 3, pp. 2550–2559, Mar. 2022.

[40] L. Ge, Y. Zhao, F. Ma, and K. Guo, "Towards longitudinal and lateral coupling control of autonomous vehicles using offset free MPC," *Control Eng. Pract.*, vol. 121, Apr. 2022, Art. no. 105074, doi: 10.1016/j.conengprac.2022.105074.

[41] D. Chu, H. Li, C. Zhao, and T. Zhou, "Trajectory tracking of autonomous vehicle based on model predictive control with PID feedback," *IEEE Trans. Intell. Transp. Syst.*, vol. 24, no. 2, pp. 2239–2250, Feb. 2022, doi: 10.1109/TITS.2022.3150365.

[42] H. Zhao, D. Sun, M. Zhao, Q. Pu, and C. Tang, "Combined longitudinal and lateral control for heterogeneous nodes in mixed vehicle platoon under V2I communication," *IEEE Trans. Intell. Transp. Syst.*, vol. 23, no. 7, pp. 6751–6765, Jul. 2022, doi: 10.1109/TITS.2021.3061413.

[43] J. Guo, Y. Luo, and K. Li, "Adaptive fuzzy sliding mode control for coordinated longitudinal and lateral motions of multiple autonomous vehicles in a platoon," *Sci. China Technol. Sci.*, vol. 60, no. 4, pp. 576–586, Apr. 2017.

[44] J. Guo, Y. Luo, and K. Li, "Adaptive coordinated leader–follower control of autonomous over-actuated electric vehicles," *Trans. Inst. Meas. Control*, vol. 39, no. 12, pp. 1798–1810, Dec. 2017.

[45] M. Goli, "Vehicle platooning: Multi-vehicle merging and control," Ph.D. dissertation, George Washington Univ., Washington, DC, USA, 2019, Art. no. 13420305.

[46] M. Goli and A. Eskandarian, "A nonlinear model predictive control design for autonomous multivehicle merging into platoons," *SAE Int. J. Transp. Saf.*, vol. 10, no. 1, pp. 73–91, Oct. 2021.

[47] M. Svec, S. Iles, and J. Matusko, "Model predictive control of vehicle dynamics based on the Koopman operator with extended dynamic mode decomposition," in *Proc. 22nd IEEE Int. Conf. Ind. Technol. (ICIT)*, Valencia, Spain, Mar. 2021, pp. 68–73.

[48] M. Korda and I. Mezić, "Linear predictors for nonlinear dynamical systems: Koopman operator meets model predictive control," *Automatica*, vol. 93, pp. 149–160, Jul. 2018.

[49] V. Cibulka, T. Haniš, M. Korda, and M. Hromcík, "Model predictive control of a vehicle using Koopman operator," *IFAC-PapersOnLine*, vol. 53, no. 2, pp. 4228–4233, 2020.

[50] E. Ling, L. Zheng, L. J. Ratliff, and S. Coogan, "Koopman operator applications in signalized traffic systems," *IEEE Trans. Intell. Transp. Syst.*, vol. 23, no. 4, pp. 3214–3225, Apr. 2022.

[51] J. L. Proctor, S. L. Brunton, and J. N. Kutz, "Dynamic mode decomposition with control," *SIAM J. Appl. Dyn. Syst.*, vol. 15, no. 1, pp. 142–161, Jul. 2016.

[52] S. Yu, E. Sheng, Y. Zhang, Y. Li, H. Chen, and Y. Hao, "Efficient nonlinear model predictive control of automated vehicles," *Mathematics*, vol. 10, no. 21, p. 4163, Nov. 2022.

[53] X. Chen, B. Zhou, and X. Wu, "Autonomous vehicle path tracking control considering the stability under lane change," *Proc. Inst. Mech. Eng., I, J. Syst. Control Eng.*, vol. 235, no. 8, pp. 1388–1402, Sep. 2021.

[54] Y. Yang, F. Ma, J. Wang, S. Zhu, S. Y. Gelbal, O. K. Torris, B. A. Guvenc, and L. Guvenc, "Cooperative ecological cruising using hierarchical control strategy with optimal sustainable performance for connected automated vehicles on varying road conditions," *J. Cleaner Prod.*, vol. 275, pp. 1–15, Dec. 2020.

[55] J. Zhan, Z. Ma, and L. Zhang, "Data-driven modeling and distributed predictive control of mixed vehicle platoons," *IEEE Trans. Intell. Vehicles*, vol. 8, no. 1, pp. 572–582, Jan. 2023, doi: 10.1109/TIV.2022.3168591.

[56] M. Kamb, E. Kaiser, S. L. Brunton, and J. N. Kutz, "Time-delay observables for koopman: Theory and applications," *SIAM J. Appl. Dyn. Syst.*, vol. 19, no. 2, pp. 886–917, Jan. 2020.

[57] D. Swaroop and J. K. Hedrick, "Constant spacing strategies for platooning in automated highway systems," *J. Dyn. Syst., Meas., Control*, vol. 121, no. 3, pp. 462–470, Sep. 1999.

[58] H. Pham, "Combined lateral and longitudinal control of vehicles for the automated highway systems," Ph.D. dissertation, Univ. California, Berkeley, CA, USA, 1996, Art. no. 9723147.

[59] S. Boyd, L. El Ghaoui, E. Feron, and V. Balakrishnan, *Linear Matrix Inequalities in System and Control Theory*, vol. 15. Philadelphia, PA, USA: SIAM, 1994.

[60] S. Yu, Y. Feng, J. Kim, and H. Chen, "Computation of terminal set for nonlinear model predictive control," *Acta Autom. Sin.*, vol. 48, no. 1, pp. 144–151, Jan. 2022.

[61] J. Ploeg, E. Semsar-Kazerooni, G. Lijster, N. van de Wouw, and H. Nijmeijer, "Graceful degradation of cooperative adaptive cruise control," *IEEE Trans. Intell. Transp. Syst.*, vol. 16, no. 1, pp. 488–497, Feb. 2015.

[62] E. Bernardi, H. Pipino, C. A. Cappelletti, and E. J. Adam, "Adaptive predictive control for industrial processes," in *Proc. 19th Workshop Inf. Process. Control (RPIC)*, San Juan, Argentina, Nov. 2021, pp. 1–6, doi: 10.1109/RPIC53795.2021.9648446.

[63] J. Luo, D. He, W. Zhu, and H. Du, "Multiobjective platooning of connected and automated vehicles using distributed economic model predictive control," *IEEE Trans. Intell. Transp. Syst.*, vol. 23, no. 10, pp. 19121–19135, Oct. 2022.

[64] E. Alcala, V. Puig, and J. Quevedo, "LPV-MPC control for autonomous vehicles," *IFAC-PapersOnLine*, vol. 52, no. 28, pp. 103–113, Nov. 2019.

[65] H. Chen and F. Allgöwer, "A quasi-infinite horizon nonlinear model predictive control scheme with guaranteed stability," *Automatica*, vol. 34, no. 10, pp. 1205–1217, 1998.

[66] J. B. Rawlings, D. Q. Mayne, and M. Diehl, *Model Predictive Control: Theory, Computation, and Design*. Madison, WI, USA: Nob Hill Publishing, 2017.

[67] S. Yu, M. Reble, H. Chen, and F. Allgöwer, "Inherent robustness properties of quasi-infinite horizon nonlinear model predictive control," *Automatica*, vol. 50, no. 9, pp. 2269–2280, Sep. 2014.

[68] J. Shen and D. Hong, "Optimal linearization via quadratic programming," *IEEE Robot. Autom. Lett.*, vol. 5, no. 3, pp. 4572–4579, Jul. 2020.

[69] Y. Lian, Y. Jiang, D. F. Opila, and C. N. Jones, "A proximal-point Lagrangian based parallelizable nonconvex solver for bilinear model predictive control," 2022, *arXiv:2206.10425*.

[70] P. Krupa, R. Jaouani, D. Limon, and T. Alamo, "A sparse ADMM-based solver for linear MPC subject to terminal quadratic constraint," 2021, *arXiv:2105.08419*.

[71] S. E. Li, K. Li, R. Rajamani, and J. Wang, "Model predictive multi objective vehicular adaptive cruise control," *IEEE Trans. Control Syst. Technol.*, vol. 19, no. 3, pp. 556–566, May 2011.

[72] B. Gao, K. Cai, T. Qu, Y. Hu, and H. Chen, "Personalized adaptive cruise control based on online driving style recognition technology and model predictive control," *IEEE Trans. Veh. Technol.*, vol. 69, no. 11, pp. 12482–12496, Nov. 2020.

[73] D. L. Luu, C. Lupu, H. Alshareefi, and H. T. Pham, "Coordinated throttle and brake control for adaptive cruise control strategy design," in *Proc. 23rd Int. Conf. Control Syst. Comput. Sci. (CSCS)*, Bucharest, Romania, May 2021.

[74] R. Kianfar, P. Falcone, and J. Fredriksson, "A distributed model predictive control approach to active steering control of string stable cooperative vehicle platoon," *IFAC Proc. Volumes*, vol. 46, no. 21, pp. 750–755, 2013.

[75] M. Zanon, J. V. Frasch, M. Vukov, S. Sager, and M. Diehl, "Model predictive control of autonomous vehicles," in *Optimization and Optimal Control in Automotive Systems*, vol. 455. Cham, Switzerland: Springer, Mar. 2014, pp. 41–57.

Yangyang Feng received the M.S. degree in control science and engineering from Jilin University, China, in 2019, where he is currently pursuing the Ph.D. degree with the Department of Control Science and Engineering. His main research interests include distributed model predictive control and control of vehicle platoons.

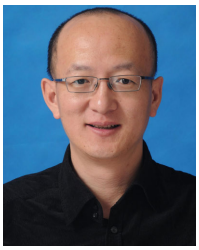

Shuyou Yu (Member, IEEE) received the Ph.D. degree in engineering cybernetics from the University of Stuttgart, Germany, in 2011. He is currently a Professor with the Department of Control Science and Engineering, Jilin University. His current research interests include model predictive control, robust control, and its applications in mechatronic systems.

Encong Sheng received the B.E. degree from the College of Communication Engineering, Jilin University, China, in 2020. He is currently pursuing the M.S. degree with the Department of Control Science and Engineering, Jilin University. His research interests include model predictive control and Koopman operator.

Yongfu Li (Senior Member, IEEE) received the Ph.D. degree in control science and engineering from Chongqing University, Chongqing, China, in 2012. He is currently a Professor with the College of Automation, Chongqing University of Posts and Telecommunications. His research interests include automated driving and intelligent transportation systems.

Shuming Shi received the Ph.D. degree in vehicle operation engineering from Jilin University in 1998. He is currently a Professor with the College of Transportation, Jilin University. His research interests include nonlinear vehicle dynamics and vehicle control systems.

Jianhua Yu received the B.E. degree from Tsinghua University, China, in 1989, and the M.S. degree in internal combustion engine from the Beijing Institute of Technology, China, in 1997. He is currently with Dongfeng Commercial Vehicle Technology Center.

Hong Chen (Fellow, IEEE) received the Ph.D. degree in system dynamics and control engineering from the University of Stuttgart, Stuttgart, Germany, in 1997. She is currently a Professor with the College of Electronics and Information Engineering, Tongji University, and a Tangaoqing Joint Professor with Jilin University. Her current research interests include model predictive control, nonlinear control, and automotive control.